A selective LIS1 requirement for mitotic spindle assembly discriminates distinct T-cell division mechanisms within the T-cell lineage

Jérémy Argenty[1], Nelly Rouquié[1], Cyrielle Bories[1], Suzanne Mélique[1], Valérie Duplan[1], Abdelhadi Saoudi[1], Nicolas Fazilleau[1], Renaud Lesourne[1]

[1] Toulouse Institute for Infectious and Inflammatory Diseases (Infinity), INSERM UMR1291, CNRS UMR5051, University Toulouse III, Toulouse, France.

Correspondence should be addressed to R.L.

Email: renaud.lesourne@inserm.fr

Abstract

The ability to proliferate is a common feature of most T-cell populations. However, proliferation follows different cell-cycle dynamics and is coupled to different functional outcomes according to T-cell subsets. Whether the mitotic machineries supporting these qualitatively distinct proliferative responses are identical remains unknown. Here, we show that disruption of the microtubule-associated protein LIS1 leads to proliferative defects associated with a blockade of T-cell development after β-selection and of peripheral CD4+ T cell expansion after antigen priming. In contrast, cell divisions in CD8+ T cells occurred independently of LIS1 following T-cell antigen receptor stimulation, although LIS1 was required for proliferation elicited by pharmacological activation. In thymocytes and CD4+ T cells, LIS1-deficiency did not affect signaling events leading to activation but led to an interruption of proliferation after the initial round of division and to p53-induced cell death. Proliferative defects resulted from a mitotic failure, characterized by the presence of extra-centrosomes and the formation of multipolar spindles, causing abnormal chromosomes congression during metaphase and separation during telophase. LIS1 was required to stabilize dynein/dynactin complexes, which promote chromosome attachment to mitotic spindles and ensure centrosome integrity. Together, these results suggest that proliferative responses are supported by distinct mitotic machineries across T-cell subsets.

Introduction

Proliferation enables the expansion, differentiation and maintenance of T cells at different stages of their life cycle. It is required for the rapid growth of antigen specific T cells, which is important for efficient control of infection. In this context, the initiation of cell division is primarily driven by signals triggered by the T-cell antigen receptor (TCR), which recognizes self or foreign peptides bound to the major histocompatibility complex (pMHC) at the surface of antigen presenting cells (APCs). Proliferation is also important during T cell development as it enables the expansion of immature CD4-CD8- thymocytes (referred to as double-negative [DN] thymocytes) that have successfully rearranged the TCR β-chain and their differentiation into CD4+CD8+ thymocytes (referred to as double-positive [DP] thymocytes) (1, 2). At these stages, proliferation is mainly driven by coordinated signaling events triggered by the pre-TCR and by the Notch receptor (3, 4). Slow proliferative events are also induced in peripheral T cells to maintain a functional and diversified pool of lymphocytes. Such homeostatic proliferation is triggered in response to TCR stimulation by self-pMHC ligands and to specific cytokines (5).

CD4+ T helper cells and CD8+ cytotoxic T cells harbor different proliferative characteristics in response to TCR stimulation. CD4+ T cells require repeated TCR stimulation to efficiently divide and show a relatively restricted expansion rate following antigen priming, while CD8+ T cells divide rapidly after single TCR stimulation (6, 7). Cell division is associated to the acquisition of effector function in CD8+ T cells (8, 9). The fate decision between the effector and memory lineages in CD8+ T cells has been proposed to occur as early as the first round of division through asymmetric divisions (9), which enables the unequal partitioning of cell fate determinants in daughter cells (8). The role of cell division in the acquisition of CD4+ T cells effector function has been controversial (10, 11). Asymmetric divisions were also reported in

CD4+ T cells (12, 13), but the contribution of such processes to T helper lineage diversification, which primarily depends on cytokine stimuli, remains also debated (14). Together, these findings suggest that different cell division dynamics and organization might govern proliferation in CD4+ and CD8+ T cells to ensure different functional outcomes. Whether the mitotic machinery supporting these qualitatively distinct proliferative responses are identical is unknown.

Lissencephaly gene 1 (LIS1, also known as PAFAHB1) is a dynein-binding protein which has important function during brain development (15). LIS1 is involved in the proliferation and migration of neural and hematopoietic stem cells (16-18). It binds to the motor protein complex dynein and regulates the dynamic of its interaction with microtubules (15, 19, 20), as well as its ability to form active complex with the multimeric protein complex dynactin (21-23). Those complexes are required for the long transport of cargos toward the minus end of microtubules (24-27) and are important for a wide variety of cellular processes, including the accumulation of γ-tubulin at the centrosome (28, 29) and the efficient formation of mitotic spindle poles during metaphases (30). Recently, we identified LIS1 as a binding partner of the T-cell signaling protein THEMIS (31, 32), which is important for thymocyte positive selection, suggesting that LIS1 could exhibit signaling function during T-cell development. LIS1 is required in several cellular models for chromosome congression and segregation during mitosis and for the establishment of mitotic spindle pole integrity (33). However, the impact of LIS1-deficiency on cell division varies according to cell types and stimulatory contexts. For example, LIS1 is essential to symmetric division of neuroepithelial stem cells prior neurogenesis, whereas LIS1-deficiency has a moderate impact on asymmetric division associated to the differentiation neuroepithelial stem cells in neural progenitors (16). Previous studies also suggest that LIS1 is dispensable for the expansion of CD8+ T cells induced following antigen

89 priming (34). Together, these findings suggest that LIS1 could have stage- or subset-specific
90 effects on T-cell mitosis, which might discriminate distinct cellular outcomes.
91
92 Here, we selected LIS1 as a candidate molecule to explore whether T-cell proliferative
93 responses could be supported by distinct mitotic machineries across different T-cell subsets,
94 such as immature thymocytes as well as CD4+ and CD8+ T cells. Using different *Cre* inducible
95 models, we identified a selective LIS1-requirement for mitosis in thymocytes and peripheral
96 CD4+ T cells following β-selection and antigen priming, respectively. In contrast, the
97 disruption of LIS1 had little impact on CD8+ T cell proliferation mediated by the TCR. In
98 thymocytes and CD4+ T cells, LIS1 deficiency led to a disruption of dynein-dynactin
99 complexes, which was associated with a loss of centrosome integrity and with the formation of
100 multipolar spindles. These mitotic abnormalities conducted to abnormal chromosomes
101 congression and separation during metaphase and telophase, and to aneuploidy and p53 up-
102 regulation upon cell division. Together, our results suggest that the mechanisms that support
103 mitosis within the T-cell lineage could vary across T-cell subsets according to the functional
104 outcomes to which they are coupled.

Results

Lis1 deficiency leads to an early block of T- and B-cell development

To evaluate the role of LIS1 during T cell development, we conditionally disrupt *Pafah1b1*, the gene encoding LIS1, using a Cre recombinase transgene driven by the human *Cd2*, which is up-regulated in T- and B-cell progenitors (35). Analysis of CD4 and CD8 surface staining in the thymus shows that the loss of LIS1 in the *Cd2-Cre* model leads to a major block of thymocyte maturation at the transition from the DN stage to the DP stage, which is associated with a strong decrease in DP, CD4 and CD8 single-positive [SP] thymocytes numbers but normal numbers of DN thymocytes (Figure 1A). Numbers of peripheral CD4+ and CD8+ T cells were also dramatically decreased in *Cd2-Cre Lis1*$^{flox/flox}$ mice compared to that in control *Lis1*$^{flox/flox}$ mice (Figure 1 – Figure Supplement 1A). Analysis of CD25 and CD44 surface staining on DN thymocytes showed that the numbers of DN4 (CD25-CD44-) thymocytes were strongly decreased in LIS1-deficient mice whereas the numbers of DN3 (CD25+CD44-) and DN2 (CD25+CD44+) thymocytes were increased, pointing-out a defect at the transition from the DN3 to the DN4 stages (Figure 1B). The percentages and numbers of thymocyte in each subsets were comparable to control mice in *Cd2-Cre Lis1*$^{flox/+}$ mice, indicating that LIS1 hemi-zygote expression is sufficient to promote T-cell development (Figure 1 – Figure Supplement 1B). Lower numbers of B cells were also detected in LIS1-deficient mice (Figure 1 – Figure Supplement 1A). Analysis of B cell development in the bone marrow indicates a strong decrease of the numbers of B220+CD19+ pro-B (IgM-c-kit+), pre-B (IgM-c-kit-) and immature B cells (IgM+c-kit-), whereas numbers of pre-pro-B cells (B220+CD19-) were normal, suggesting a defect of maturation of pre-pro-B cells into pro-B cells (Figure 1 – Figure

Supplement 1C). Together, these data indicate that LIS1 is essential for early stages of T- and B-cell development.

LIS1 is required for thymocyte proliferation after the β-selection checkpoint

One critical developmental step at the DN3 to DN4 transition is the formation of a functional TCR β chain, which associates with the pTα chain upon successful rearrangement to form the pre-TCR. Pre-TCR formation triggers signaling events which lead to the up-regulation of CD5 and, together with Notch and the IL-7 receptor (IL-7R) stimulation, to the initiation of several division cycles and to further maturation of thymocytes into DN4 thymocytes (1, 2, 4, 36, 37). The percentages of DN3 thymocytes that express the TCRβ chain and CD27, a cell surface maker of the β-selection checkpoint (38), were lower in *Cd2-Cre Lis1*$^{flox/flox}$ mice as compared those that in control mice expressing LIS1, suggesting that LIS1 might be important for the rearrangement of the TCRβ chain and/or for the expansion of cells that successfully rearranged the TCRβ chain (Figure 1C). The expression level of CD5 was slightly increased in *Cd2-Cre Lis1*$^{flox/flox}$ DN3 thymocytes compared to that in *Lis1*$^{flox/flox}$ DN3 cells, whereas IL-7R cell surface levels was not affected by LIS1 expression, suggesting that LIS1 was not required for functional pre-TCR assembly but rather for the expansion of DN3 thymocytes after the β-selection checkpoint (Figure 1D and 1E). Notch signaling leads to increase cell sizes of thymocyte after β-selection and to the up-regulation of the transferrin receptor CD71 (39, 40). The loss of LIS1 did not affect these two parameters, suggesting that LIS1 is dispensable for Notch-mediated signaling (Figure 1E). To evaluate whether LIS1 is important for the proliferation of DN3 thymocytes following the β-selection checkpoint, we quantified DN cells that have duplicated DNA copies prior and after the β-selection checkpoint. Thymocytes with duplicated DNA copies could not be detected prior the β-selection checkpoint in wild-type and

LIS1-deficient mice (Figure 1F). Approximately 10% of thymocytes were in the G2/M phase of cell cycle after β-selection in wild-type mice whereas this proportion rose to 20% in LIS1-deficient mice, suggesting a possible failure of LIS1-deficient thymocytes to successfully complete division cycles (Figure 1F).

To directly address this hypothesis, we analyzed the proliferation of DN3 thymocytes upon stimulation with OP9-Dl1 cells, a bone-marrow-derived stromal cell line that ectopically expresses the Notch ligand, Delta-like 1 (Dl1), and which induces efficient T-cell lymphopoiesis from the DN stages to the DP stage (41). We observed that the percentages of cells that proliferate in response to OP9-Dl1 stimulation were strongly decreased in the absence of LIS1 (Figure 2A). This was associated with a failure of DN3 cells to effectively differentiate into CD25-CD44- DN4 cells (Figure 2B). The TCRβ chain and the receptor CD5 were up-regulated normally after stimulation, indicating that the defect in proliferation was not the consequence of defects in stimulatory signals required for proliferation and differentiation (Figure 2C). The loss of LIS1 also did not affect the expression of CD71 (Figure 2D) and Bcl-2 (Figure 2E), which depends on Notch and IL-7R signaling respectively (42, 43), suggesting that LIS1 does not operate downstream of these receptors. By contrast, cell cycle analysis showed that the loss of LIS1 led to a strong accumulation of cells at the G2/M stage, indicative of ineffective division processes after the DNA duplication phase (Figure 2F). Together, those results suggest that LIS1 controls cellular events that are required for the efficient division of thymocytes after the β-selection checkpoint.

LIS1 is required for TCR-mediated proliferation in CD4+ T cells

Previous studies suggested that LIS1-deficient CD4+ and CD8+ T cells fail to proliferate in response to cytokine-driven homeostatic signals but successfully divide in response to TCR cross-linking *in vitro* or following infection with a *Listeria monocytogenes* strain expressing ovalbumin (34). Since the loss of LIS1 had such a strong impact on thymocyte proliferation following pre-TCR stimulation, we decided to compare the role of LIS1 in the proliferation of CD4+ and CD8+ T cells in response to TCR engagement.

To examine the role of LIS1 in peripheral T cells, we conditionally disrupt *Pafah1b1* using a Cre recombinase transgene driven by the *Cd4* promoter, which is up-regulated at the DP stage after the proliferation step of DN3-DN4 thymocytes. We observed that the loss of LIS1 at this stage of development did not affect the percentages and numbers of DN, DP and SP thymocytes (Figure 3 – Figure Supplement 1A). Normal numbers of mature $TCR^{hi}CD24^{low}$ SP thymocytes were also generated in the absence of LIS1 (Figure 3 – Figure Supplement 1B). The maturation of DP thymocytes into TCR^{hi}CD4 SP thymocytes occurred also normally in *Cd4-Cre Lis1*$^{flox/flox}$ mice expressing a fixed MHC class II–restricted αβ-TCR transgene (AND), suggesting that LIS1 is not essential for positive selection (Figure 3 – Figure Supplement 1C). As previously reported in a similar conditional knockout model (34), the deletion of LIS1 led to a dramatic decrease of peripheral CD4+ and CD8+ T cells numbers (Figure 3 – Figure Supplement 1D). This defect was previously imputed to a reduced ability of CD4+ and CD8+ T cells to proliferate in response to cytokine-driven homeostatic signals (34). In contrast, the mono-allelic deletion of LIS1 in *Cd4-Cre Lis1*$^{flox/+}$ did not affect the numbers of CD4+ and CD8+ T cells (Figure 3 – Figure Supplement 1E), suggesting that reduced LIS1 dosage does not affect T-cell homeostasis.

We next evaluated the effect of LIS1 deficiency on the proliferation of CD4+ and CD8+ T cells following TCR stimulation. We observed that the percentages of proliferating CD4+ T cells were strongly decreased in the absence of LIS1 following TCR stimulation (Figure 3A). The analysis of cell percentages in each division cycle showed that LIS1-deficient CD4+ T cells successfully performed the first cycle of division but failed to divide further and accumulated at this stage (Figure 3A). Similar results were obtained following stimulation with Phorbol 12-myristate 13-acetate (PMA) and ionomycin, indicating that LIS1-dependent effects on CD4+ T-cell proliferation were not dependent on proximal TCR signaling events (Figure 3A). In contrast, mono-allelic deletion of the LIS1 encoding gene did not affect the rate of proliferating CD4+ T cells following TCR stimulation (Figure 3 – Figure Supplement 2A). Activation markers such as CD25 and CD69 were also up-regulated normally in the absence of LIS1, indicating that more distal TCR signaling events were not affected by LIS1 deficiency (Figure 3B). Cell cycle analysis show that CD4+ T cells with duplicated DNA copies accumulated in LIS1-deficient T cells as compared to that in control cells following stimulation (Figure 3C). Contrasting with the strong effect observed on CD4+ T cell proliferation, the loss of LIS1 had a rather modest impact on the total fraction of CD8+ T cells that proliferate in response to TCR cross-linking and on the fraction of cells that had successfully divided after the first division cycle (Figure 3D). The loss of LIS1 also did not result in the accumulation of CD8+ T cells with duplicated DNA copies (Figure 3C). LIS1 was not detected in cell extracts from both CD4+ and CD8+ T cells from *Cd4-Cre Lis1*$^{flox/flox}$ mice, indicating that the mild impact of LIS1 on CD8+ T cell proliferation was not the consequence of the remaining expression of LIS1 in this subset (Figure 3 – Figure Supplement 2B). Also, the stimulation of CD8+ T cells with PMA and ionomycin led to an important decrease of the total fraction of proliferating T cells, suggesting that cell divisions in CD8+ T cells are controlled by different mechanisms, which vary according to their LIS1-dependency based on the context of stimulation.

227

228 To determine whether LIS1 controls the proliferation of CD4+ T cells in response to antigen
229 stimulation *in vivo*, we crossed *Cd4-Cre Lis1*$^{flox/flox}$ mice with transgenic mice expressing the
230 allotypic marker CD45.1 and the class-II restricted OT2 TCR specific for the chicken
231 ovalbumin 323-339 peptide. CD4+ T cells from OT2+ *Cd4-Cre Lis1*$^{flox/flox}$ and *Lis1*$^{flox/flox}$ mice
232 were stained with CellTrace violet (CTV) and injected into C57Bl/6 mice expressing the
233 allotypic marker CD45.2+. Mice were next immunized with ovalbumin and CD45.1+CD4+ T
234 cells were analyzed in the spleen at day two, three and seven after immunization. The numbers
235 of LIS1-deficient CD45.1+ CD4+ T cells in the spleen were similar to those of control cells at
236 day two after immunization, indicating that the loss of LIS1 did not affect the ability of CD4+
237 T cells to migrate into the spleen (Figure 3E). At this stage, the percentages of divided cells
238 were very low and were not significantly different according to LIS1 expression. At day three
239 after immunization, we observed a large fraction of divided *Lis1*$^{flox/flox}$ CD45.1+CD4+ T cells,
240 with the majority of cells having completed more than two rounds of division (Figure 3E and
241 3F). By contrast, the fraction of divided cells was strongly decreased in the absence of LIS1
242 with almost a complete failure of those cells to engage more than one division cycle (Figure 3E
243 and 3F). Numbers of LIS1-deficient CD4+CD45.1+ T cells were strongly decreased compared
244 to control CD4+CD45.1+ T cells that express LIS1 (Figure 3E). Of note, the expression level
245 of CD44 on undivided CD4+CD45.1+ T cells was similar whether or not LIS1 was expressed,
246 suggesting that LIS1 was not required for CD4+ T-cell activation *in vivo* (Figure 3F). The loss
247 of LIS1 also resulted in a marked decrease in the percentages and numbers of CD4+CD45.1+
248 T cells at day seven after immunization (Figure 3 – Figure Supplement 2C). Together, these
249 results suggest that CD4+ and CD8+ T cells engage distinct cell division mechanisms upon
250 antigen priming that diverge in their requirement for LIS1.

251

252 **LIS1-dependent control of chromosome alignment during metaphase is required for**
253 **effective mitosis**
254
255 We next aimed to more precisely characterize the role of LIS1 during the division of CD4+ T
256 cells. Our data suggest a block either at the G2 or the M phase of cell cycle in LIS1-deficient
257 thymocytes and CD4+ T cells (Figure 1E, Figure 2E and Figure 3C). We used image stream
258 flow cytometry to discriminate cells with duplicated DNA copies that contain chromosomes (in
259 M phase) from cells that have uncondensed DNA (in G2 phase). *Cd4-Cre Lis1*$^{flox/flox}$ *and*
260 *Lis1*$^{flox/flox}$ CD4+ T cells were stimulated for 48 hours with anti-CD3 and anti-CD28 antibodies
261 and stained with DAPI. Analysis were next performed on cells with duplicated DNA copies.
262 The Bright Detail Intensity (BDI) feature on the DAPI channel, which evaluates areas of peak
263 fluorescence intensity after subtraction of background fluorescence, was selected for its ability
264 to automatically discriminate cells in M and G2 phases, as illustrated in Figure 4A. The
265 percentages of mitotic CD4+ T cells were increased in the absence of LIS1, suggesting that
266 LIS1-deficient CD4+ T cells fail to complete mitosis. To determine more precisely the stage of
267 mitosis at which this defect occurs, we analyzed whether LIS1 was required for cells to
268 successfully reach metaphase. *Cd4-Cre Lis1*$^{flox/flox}$ *and Lis1*$^{flox/flox}$ CD4+ T cells were stimulated
269 for 48 hours with anti-CD3 and anti-CD28 antibodies and synchronized with nocodazole for 18
270 hours prior treatment with MG132 to induce metaphase arrest. The percentages of cells in
271 metaphase were evaluated by image stream flow cytometry using the "Elongatedness"
272 parameter, which calculates the length to width ratios (L/W) on pre-defined DAPI masks.
273 CD4+ T cells with L/W ratios superior to 1.5 show aligned chromosomes patterns
274 representative of metaphase (Figure 4B). This analysis showed that the percentages of cells,
275 which successfully reached metaphase were strongly reduced in the absence of LIS1 (Figure
276 4B). To more precisely characterized mitotic events that could be affected by LIS1-deficiency,

we next analyzed the course of mitosis in *Cd4-Cre Lis1*$^{flox/flox}$ *and Lis1*$^{flox/flox}$ CD4+ T cells by time-lapse microscopy. We observed that both *Cd4-Cre Lis1*$^{flox/flox}$ *and Lis1*$^{flox/flox}$ CD4+ T cells successfully condensated their DNA to form chromosomes (Figure 4C, video 1, 2 and 3). However, chromosomes remained disorganized in *Cd4-Cre Lis1*$^{flox/flox}$ CD4+ T cells and failed to segregate rapidly after condensation as compared to those in control cells (Figure 4C). At the final step of mitosis, LIS1-deficient CD4+ T cells either failed to divide (Figure 4C, 4D and video 2) or divided with an apparent unequal repartition of chromosomes in daughter cells (Figure 4C, 4D and video 3), which was associated with the formation of multiple nuclei or multilobed nuclei (Figure 4C and video 2). Confirming the observations based on time-lapse microscopy, quantitative analysis on G2 cells selected by image stream showed that the percentages of cells with multiple nuclei were strongly increased in the absence of LIS1 (Figure 4E).

The abnormal repartition of chromosomes in daughter cells, so called aneuploidy, is generally associated with the up-regulation of the tumor suppressor p53, which contributes to eliminate cells through apoptotic processes prior the emergence of possible oncogenic transformation (44). To determine whether impaired mitosis associated to LIS1-deficiency leads to apoptosis, we analyzed the percentages of apoptotic cells in undivided and divided peripheral CD4+ T cells following stimulation with anti-CD3 and anti-CD28 antibodies for 48 hours. We observed that the loss of LIS1 was associated with increased frequency of apoptotic cells among divided cells, but had no significant effect on apoptosis in activated CD25+ undivided cells (Figure 5A). Analysis of p53 expression prior the initial cycle of division at 24 hours, showed comparable expression level of p53 between wild-type and LIS1-deficient cells, whereas p53 expression was dramatically increased in LIS1-deficient CD4+ T cells as compared to that in control cells after the initial division cycles at 48 hours (Figure 5B). In comparison, the

abundance of p53 after 48 hours of stimulation was comparable in wild-type and LIS1-deficient CD8+ T cells, supporting that the loss of LIS1 has a modest impact on cell division in the CD8+ lineage (Figure 5B). Analysis was next performed on DN3 thymocytes stimulated with OP9-Dl1 cells and led to a similar increase of apoptosis exclusively in divided thymocytes from LIS1-deficient mice (Figure 5C). The expression level of p53 was also strongly increased in total LIS1-deficient DN3 thymocytes as compared to that in wild-type DN3 cells (Figure 5D). Altogether, those results indicate that the loss of LIS1 results in a defective chromosomes congression and separation during metaphase, which leads to aneuploidy, to the up-regulation of p53 and to the development of apoptotic program.

LIS1 controls mitotic spindle and centrosome integrity in CD4+ T cells by promoting the formation of dynein-dynactin complexes

Each spindle pole is normally established by one centrosome containing a pair of centrioles embedded in the pericentriolar material (PCM) containing γ-tubulin ring complexes (γ-TuRCs) from which microtubules nucleate. Centrosomes replicate once every cell cycle during the G1-S phase (45). Anomaly in centrosomes replication and PCM fragmentation may lead to the formation of extra-centrosomes which can be associated to the formation of multipolar spindles and to the unequal repartition of chromosomes (46, 47). Previous studies in embryonic fibroblast show that the loss of LIS1 is associated with the formation of multipolar spindle due to the formation of extra-centrosomes (33). However, this defect is not systematically observed in the absence of LIS1. For instance, the loss of LIS1 in hematopoietic stem cells has a moderate effect on the integrity of the mitotic spindle but rather affects the spindle positioning during telophase, leading to increased rate of asymmetric divisions (18).

To evaluate whether the loss of LIS1 could be associated with an aberrant number of centrosomes or to a loss of centrosome integrity prior the division of CD4+ T cells, we stimulated CTV stained CD4+ T cells from *Cd4-Cre Lis1$^{flox/flox}$ and Lis1$^{flox/flox}$* mice with anti-CD3 and anti-CD28 antibodies for 48 hours and FACS sorted undivided CTV^{hi} cells based on the forward-size-scattered parameter to discriminate unactivated (forward-scatter [FSC]^{lo}) from activated (FSC^{hi}) cells. Cells were analyzed by confocal microscopy after γ-tubulin and DAPI staining. In the presence of LIS1, we observed that the vast majority of FSC^{lo} CD4+ T cells contained a single centrosome, whereas the majority FSC^{hi} cells had two centrosomes as expected from cells in mitosis (Figure 6A). In the absence of LIS1, more than 50% of mitotic FSC^{hi} CD4+ T cells had more than two centrosomes (Fig. 6A). The loss of LIS1 did not affect centrosome copy numbers in unactivated CD4+ T cells (Figure 6A), indicating that LIS1 is engaged following TCR stimulation once the cell cycle has started, possibly at the stage of centrosome duplication. Some extra-centrosomes showed reduced accumulation of γ-tubulin as compared to normal centrosomes in wild-type cells, suggesting that the loss of LIS1 leads to PCM fragmentation or to the loss of centrosome integrity rather than centrosome supernumerary duplication (Figure 6B). Analysis of γ- and α-tubulin stainings in LIS1-deficient CD4+ T cells show that these extra-centrosomes were "active" in that they could effectively nucleate microtubule fibers (Figure 6B). Multiple centrosomes were also observed in cells sorted post-β-selection DN3 thymocytes (Figure 6C). Together, these results indicate that LIS1 is required for the formation of stable bipolar mitotic spindles upon division of thymocytes and CD4+ T cells.

The biochemical basis by which LIS1 affects dynein function has been the focus of intense investigations yielding to contradictory findings and divergent models (15). Evidence from early studies suggest that LIS1 might be acting as a "clutch" that would prevent dynein's

ATPase domain from transmitting a detachment signal to its track-binding domain (20). More recent *in vitro* investigations with recombinant proteins identify critical function for LIS1 in the assembly of active dynein-dynactin complexes (21, 22). To analyze whether the cellular defect observed in LIS1-deficient CD4+ T cells could be associated with defect in dynein-dynactin complex assembly, we compared the amount of p150Glued, a subunit of the dynactin complex, that co-immunoprecipitated with the intermediate chain of dynein (DIC) in CD4+ T cells isolated from *Cd4-Cre Lis1*$^{flox/flox}$ and *Lis1*$^{flox/flox}$ mice (48). The amount of p150Glued that co-immunoprecipitated with DIC was decreased in LIS1-deficient cells as compared to wild-type controls (Figure 6D). Similar amount of the dynein heavy chain (DHC) was co-immunoprecipitated with the DIC in LIS1-deficient and wild-type cells (Figure. 6D), indicating that the defect in DIC-p150Glued interaction was not due do ineffective assembly of the dynein complex itself. These results suggest that LIS1 controls the integrity of mitotic spindle pole assembly in peripheral CD4+ T cells by stabilizing the association between dynein and dynactin complexes.

Discussion

In this study, we identified a selective LIS1-requirement for mitosis in thymocytes and peripheral CD4+ T cells following β-selection and antigen priming, respectively. LIS1-dependent proliferation defects resulted in a block of early T-cell development and in a nearly complete lack of CD4+ T-cell expansion following activation. LIS1 deficiency in thymocytes and CD4+ T cells led to a disruption of dynein-dynactin complexes, which was associated with a loss of centrosome integrity and with the formation of multipolar spindles. These mitotic abnormalities were in turn associated to abnormal chromosomes reorganization during metaphase and telophase and to aneuploidy and p53 up-regulation upon cell division. Importantly, whereas LIS1 deficiency led to a strong block of CD8+ T-cell proliferation upon PMA and ionomycin stimulation, it had very little effects, if any, on the proliferation of CD8+ T cells following TCR engagement, suggesting that the mitotic machinery that orchestrates mitosis in CD8+ T cells upon TCR stimulation is different from that engaged in thymocytes and peripheral CD4+ T cells upon pre-TCR and TCR engagement.

LIS1 was shown to be dispensable for the proliferation of antigen-specific CD8+ T cell following infection with *Listeria monocytogenes* (34), supporting the data that we report here in CD8+ T cells following TCR stimulation. Comparable cell type-specific effects of LIS1 on proliferation have been described at early stages of neurogenesis and hematopoiesis (16, 18). The loss of LIS1 in neuroepithelial stem cells leads to mitotic arrest and apoptosis upon symmetrical division events associated to progenitor cell maintenance, whereas it has only a moderate effect on asymmetrical division associated with neurogenesis, suggesting that symmetric division might be more LIS1-sensitive than asymmetric division (16). Accordingly, LIS1-deficiency leads to a dramatic decrease of proliferation when CD8+ T cells are stimulated

with soluble ligands such as cytokines and PMA/ionomycin, which favor symmetric division (34). This suggests that the different sensitivity of CD4+ and CD8+ T cells to LIS1 deficiency upon cell division is not simply the consequence of a preferential use of LIS1 in CD4+ T cells but rather the consequence of different mitotic organizations in CD4+ and CD8+ T cells in the context of polarized cell stimulations, which might exhibit different requirement for LIS1. This raises the question of whether CD4+ T cells would be more prone to symmetric divisions than CD8+ T cells. Theoretically, the experimental settings that we used in this study might not be optimal for eliciting asymmetric cell division, since we stimulated T cells with anti-CD3 and anti-CD28 in the absence of ICAM-1, which is required for asymmetric cell divisions to occur in the context of APC stimulation (8). However, the rate of asymmetric cell divisions might be less influenced by ICAM-1 stimulation in conditions where plate-bound stimulations with antibodies are used (49). Asymmetric cell divisions have been detected in CD4+ T cells after the first antigen encounter (8), but it is unknown whether these divisions occur systematically or whether they occur with variable frequencies that could be context-dependent. It is also unclear whether CD4+ and CD8+ T cells have similar rates of asymmetric division since the literature is lacking of quantitative studies in which cellular events associated to mitosis would be investigated side-by-side in those two subsets. The repartition of the transcription factor T-bet in daughter cells was compared in one study by flow cytometry in CD4+ and CD8+ T cells after a first round of cell division (12). Authors showed that T-bet segregates unequally in daughter cells in both CD4+ and CD8+ T cells. However, the disparity of T-bet between daughter cells was higher in CD8+ T cells as compared to that in CD4+ T cells (5- versus 3-fold), suggesting that cell-fate determinants are either more equally (or less unequally) distributed in daughter cells from the CD4+ lineage or that the rate of symmetric divisions is higher in CD4+ T cells than in the CD8+ T cells. More extensive analysis would be required to

precisely quantify the rate of symmetric and asymmetric cell divisions in CD4+ and CD8+ T cells in the context of APC stimulation.

Mechanistically, we show that LIS1 is important in CD4+ T cells to stabilize the interaction of the microtubule-associated motor protein dynein with the dynactin complex, which facilitates the binding of dynein to cargos and promotes thereby their transport along microtubule fibers. This is in agreement with recent *in vitro* studies showing that LIS1 is required for the efficient assembly of active dynein-dynactin complexes (21, 22). Given the pleiotropic role of the dynein-dynactin complexes during mitosis, several scenarios could possibly explain the defect of proliferation observed in thymocytes and peripheral CD4+ T cells. Two non-exclusive scenarios seem the most likely to us. A first scenario is that the loss of LIS1 leads to an inefficient attachment of the chromosome kinetochores to dynein, leading to metaphase delay and possibly to the asynchronous chromatid separation, a phenomena call “cohesion fatigue”, which leads to centriole separation and the formation of multipolar spindles (50). This possibility is supported by studies showing that LIS1 is localized to the kinetochores in fibroblasts and is required for the normal alignment of chromosomes during metaphases (33, 51) and for targeting the dynein complex to kinetochore (33). A second possibility is that the absence of LIS1 leads to the fragmentation of the PCM, which is associated with the formation of multipolar spindles and the erroneous merotelic kinetochore-microtubule attachments (a single kinetochore attached to microtubules oriented to more than one spindle pole), which can cause chromosomal instability in cells that ultimately undergo bipolar division (52). This is supported by the facts that several PCM components are transported towards centrosomes along microtubules by the dynein–dynactin motor complex (53, 54) and that the depletion of multiple pericentriolar proteins results in PCM fragmentation, which subsequently generates multipolar spindles (54-56).

We previously identified LIS1 as a binding partner of the signaling protein THEMIS in thymocytes and confirmed this interaction through yeast two-hybrid approaches (31, 32). THEMIS enhances positive selection in thymocytes (57-59) and is important for the maintenance of peripheral CD8+ T cells by stimulating cytokine-driven signals leading to homeostatic proliferation (60). Although LIS1 deficiency does not modulate the efficiency of thymocyte positive selection, the loss of LIS1 is associated with a strong defect of peripheral T cell proliferation in response to IL-2 and IL-15 stimulation (34). THEMIS and LIS1 deficiencies both lead to severely compromised CD8+ T cell proliferation following transfer in lymphopenic hosts (34, 60). Although this defect was attributed to stimulatory function of THEMIS on IL-2 and IL-15-mediated signaling, we cannot rule out the possibility that THEMIS would play a more direct role in cell cycle by controlling LIS1-mediated events. THEMIS operates by repressing the tyrosine phosphatase activity of SHP-1 and SHP-2, which are key regulatory proteins of TCR signaling (61). Gain-of-function mutations of SHP-2 in mouse embryonic fibroblast and leukemia cells lead to centrosome amplification and aberrant mitosis with misaligned chromosomes (62). Thus, the hyper activation of SHP-2 resulting from THEMIS deficiency may lead to cellular defects similar to those observed in LIS1-deficient T cells. An interesting perspective to this work would be to investigate further whether the loss of THEMIS in CD8+ T cells would lead to similar mitotic defects to those observed in LIS1-deficient thymocytes and CD4+ T cells upon TCR stimulation.

The fact that LIS1 deficiency increases the frequency of aneuploidy and leads to the up-regulation of p53 expression suggests that defects affecting LIS1 expression or function could favor oncogenic transformation in lymphoid cells. LIS1 is necessary for the extensive growth of tumor cells in some cancer models. The genetic disruption of LIS1 in hematopoietic stem

cells blocks the propagation of myeloid leukemia (18). However, several evidences suggest also that the alteration of LIS1 expression could contribute to the carcinogenesis of several cancers such as hepatocellular carcinoma (63, 64), neuroblastoma (65), glioma (66) and cholangiocarcinoma (67). Thus, although a minimal expression level of LIS1 might be mandatory for extensive tumor growth, partial deficiencies in LIS1 might favor oncogenic transformation. Although mono-allelic deficiency of LIS1 did not detectably affect CD4+ T-cell proliferation *in vitro*, the partial loss of LIS1 function may enhance the risk of aneuploidy-driven cancer in a tumor-suppressor failing context. This could be relevant in humans since genetic variants on *pafah1b1* have been associated with a higher risk to develop acute myeloid leukemia (68).

Materials and methods

Key Resources Table

Key Resources Table				
Reagent type (species) or resource	**Designation**	**Source or reference**	**Identifiers**	**Additional information**
Genetic reagent (Mus. musculus)	129S-Pafah1b1^{tm2Awb}/J	Jackson laboratories	Strain #:008002 RRID:IMSR_JAX:008002	This stain was provided by Dr. Deanna S. Smith (University of South Carolina, Columbia, USA)
Genetic reagent (Mus. musculus)	B6.Cg-Tg(CD2-icre)4Kio/J	Jackson laboratories	Strain #:008520 RRID:IMSR_JAX:008520	
Genetic reagent (Mus. musculus)	Tg(Cd4-cre)1Cwi/BfluJ	Jackson laboratories	Strain #:017336 RRID:IMSR_JAX:017336	
Cell line Mus musculus	OP9-dl1		Schmitt TM, de Pooter RF, Gronski MA, Cho SK, Ohashi PS, Zuniga-Pflucker JC. Induction of T cell development and establishment of T cell competence from embryonic stem cells differentiated in vitro. Nature immunology. 2004;5(4):410-7.	
antibody	anti-CD3ε Hamster monoclonal	Biolegend	clone 2C-11	Purified unconjugated
antibody	anti-CD28 Hamster monoclonal	Biolegend	clone 37.51	Purified unconjugated
antibody	anti-CD8α Rat monoclonal	Thermo Fisher Scientific	clone 53-6.7	Conjugated to A-700 1/300
antibody	anti-CD4 Rat monoclonal	BD Bioscience	clone RM4-5	Conjugated to Pacific Blue 1/1000
antibody	anti-CD24 Rat monoclonal	BioLegend	clone M1/69	Conjugated to PE 1/500
antibody	anti-TCRβ Hamster monoclonal	BD Bioscience	clone H57-597	Conjugated to FITC 1/400

antibody	anti-TCRβ Hamster monoclonal	Thermo Fisher Scientific	clone H57-597	Conjugated to PECy7 1/1500
antibody	anti-Vα11 Rat monoclonal	BD Bioscience	clone RR8-1	Conjugated to FITC 1/400
antibody	anti-CD5 Rat monoclonal	BD Bioscience	clone 53-7.3	Conjugated to APC 1/1000
antibody	anti-CD5 Rat monoclonal	Thermo Fisher Scientific	clone 53-7.3	Conjugated to FITC 1/1000
antibody	anti-CD69 Hamster monoclonal	BD Bioscience	clone H1.2F3	Conjugated to FITC 1/200
antibody	anti-B220 Rat monoclonal	BD Bioscience	clone RA3-6B2	Conjugated to PE 1/400
antibody	anti-Gr1 Rat monoclonal	BioLegend	clone RB6-8C5	Conjugated to PE 1/300
antibody	anti-CD11b Rat monoclonal	BioLegend	clone M1/70	Conjugated to PE 1/200
antibody	anti-CD11c Hamster monoclonal	BioLegend	clone N418	Conjugated to PE 1/200
antibody	anti-Ter119 Rat monoclonal	BioLegend	clone TER119	Conjugated to PE 1/200
antibody	anti-CD3ε Hamster monoclonal	BioLegend	clone 145-2C11	Conjugated to PE 1/200
antibody	anti-NK1.1 Mouse monoclonal	BD Bioscience	clone PK136	Conjugated to PE 1/200
antibody	anti-TCRγδ Hamster monoclonal	BD Bioscience	clone GL3	Conjugated to 1/200
antibody	anti-CD44 Rat monoclonal	Thermo Fisher Scientific	clone IM7	Conjugated to FITC 1/200
antibody	anti-CD25 Rat monoclonal	BD Bioscience	clone PC61.5	Conjugated to PercP Cy5.5 1/300
antibody	anti-CD71 Rat monoclonal	BioLegend	clone R17217	Conjugated to PeCy7 1/400
antibody	Anti-CD27 Hamster monoclonal	BD Bioscience	clone LG.3A10	Conjugated to APC 1/200
antibody	anti-IL-7R Rat monoclonal	BD Bioscience	clone A7R34	Conjugated to A700 1/500

antibody	anti-IL-7R Rat monoclonal	BD Bioscience	clone A7R34	Conjugated to APC 1/400
antibody	anti-BCL-2 Hamster monoclonal	BD Bioscience	clone 3F11	Conjugated to FITC
antibody	anti-CD19 Rat monoclonal	BioLegend	clone 1D3/CD19	Conjugated to PercPCY5.5 1/500
antibody	anti-c-kit Rat monoclonal	BioLegend	clone 2B8	Conjugated to PE 1/200
antibody	anti-c-kit Rat monoclonal	BD Bioscience	clone 2B8	Conjugated to APC 1/200
antibody	anti-IgM Rat monoclonal	BD Bioscience	clone RMM-1	Conjugated to PECy7 1/300
antibody	anti-CD45.1 Mouse monoclonal	BD Bioscience	clone A20	Conjugated to PE 1/500
antibody	anti-γ-tubulin Mouse monoclonal	Biolegend	clone 14C11	Purified unconjugated
antibody	anti-α-tubulin Mouse monoclonal	Thermo Fisher Scientific	clone DM1A	Purified unconjugated
antibody	Goat anti-Mouse IgG2b	Thermo Fisher Scientific	cat#A-21147	Alexa Fluor™ 555
antibody	anti-Dynein IC Mouse monoclonal	Santa-Cruz biotechnologies	clone 74-1	Purified unconjugated
antibody	anti-LIS1 Rabbit polyclonal	Santa-Cruz biotechnologies	sc-15319	Purified unconjugated
antibody	anti-Dynein HC Rabbit polyclonal	Santa-Cruz biotechnologies	sc-9115	Purified unconjugated
antibody	Anti-p150glued Mouse monoclonal	BD Biosciences	clone 1/p150Glued	Purified unconjugated
antibody	anti-p53 Mouse monoclonal	Cell signaling	clone 1C12	Purified unconjugated
antibody	anti-Rac1 Mouse monoclonal	Millipore	clone 23A8	Purified unconjugated
other	AnnexinV	BD bioscience	RRID: AB_2868885	APC
other	AnnexinV binding buffer	BD bioscience	Cat#556454	
other	eBioscience™ Fixable Viability Dye	Thermo Fisher Scientific	Cat#65-0865-14	eFluor™ 780 APC-H7
other	Permeabilization buffer	Thermo Fisher Scientific	Cat#00-8333-56	
other	Chambered glass coverslip	IBIDI	Cat#80821	

other	Dynabeads™ Untouched™ Mouse CD4 Cells Kit	Thermo Fisher Scientific	Cat#11415D	
other	DAPI	Sigma-Aldrich	cat#D9542	1mg/mL
other	Hoechst 33342	Sigma-Aldrich	cat#14533	50ng/ml
Other	Cell trace Violet	Thermo Fisher Scientific	cat#C34557	2 μM
Other	DABCO	Sigma Aldrich	cat#D27802	
chemical compound, drug	Nocodazole	Sigma Aldrich	cat#M1404	100ng/ml
chemical compound, drug	MG132	Sigma Aldrich	cat#M7449	10 μM
chemical compound, drug	phorbol 12-myristate 13-acetate (PMA)	Sigma Aldrich	cat#P8139	100ng/ml
chemical compound, drug	Ionomycine	Sigma Aldrich	cat#I0634	100ng/ml
chemical compound, drug	RIBI	Sigma Adjuvant System	cat#S6322	
Cytokine	Mouse IL-7	Peprotech	cat#217-17	10 ng/ml
software	IDEAS	Millipore		

Mice

Lis1$^{flox/flox}$ mice were described previously (69). These mice were bred with hCD2-cre transgenic mice (https://www.jax.org/strain/008520) in which the human *cd2* promoter directs the expression of the CRE recombinase at early stages of T and B cell development. *Lis1*$^{flox/flox}$ mice were also bred with CD4-Cre transgenic mice (https://www.jax.org/strain/017336) in which the *cd4* promoter directs the expression of the CRE recombinase during T cell development in CD4+CD8+ thymocytes. AND and OT-2 TCR-transgenic mice were from Taconic Farms. All the experiments were conducted with sex and age-matched mice between 6 and 12 weeks old housed under specific pathogen-free conditions at the INSERM animal facility (US-006; accreditation number A-31 55508 delivered by the French Ministry of

Agriculture to perform experiments on live mice). All experimental protocols were approved by a Ministry-approved ethics committee (CEEA-122) and follow the French and European regulations on care and protection of the Laboratory Animals (EC Directive 2010/63).

Antibodies

The following antibodies were used.

For stimulation and cell culture: anti-CD3ε (145-2C11) and anti-CD28 (37.51) antibodies were from Biolegend. *For cell sorting and flow cytometry analysis:* anti-CD8α (clone 53-6.7), anti-CD4 (clone RM4-5), anti-CD24 (clone M1/69), anti-TCRβ (clone H57-597), anti-Vα11 (clone RR8-1), anti-CD5 (clone 53-7.3), anti-CD69 (clone H1.2F3), anti-B220 (clone RA3-6B2), anti-Gr1 (clone RB6-8C5), anti-CD11b (clone M1/70), anti-CD27 (clone LG.3A10), anti-CD11c (clone N418), anti-Ter119 (clone TER119), anti-CD3 (clone 145-2C11), anti-NK1.1 (clone PK136), anti-TCRγδ (clone GL3), anti-CD44 (clone IM7), anti-CD25 (clone PC61.5), anti-CD71 (clone R17217), anti-IL-7R (clone A7R34), anti-BCL-2 (clone 3F11), anti-CD19 (clone 1D3/CD19), anti-c-kit (clone 2B8), anti-IgM (clone RMM-1) and anti-CD45.1 (clone A20) were from BD Bioscience and Biolegend. *For imaging studies:* anti-γ-tubulin (clone 14C11) was from Biolegend and anti-α-tubulin (DM1A) was from (Thermo Fisher Scientific). *For immunoprecipitation and Western blot analysis:* anti-DIC (clone 74-1), IgG2b isotype control (sc-3879), anti-LIS1 (sc-15319), anti-DHC (sc-9115) were from Santa-Cruz biotechnologies. Anti-p150glued (clone 1/p150Glued) were from BD Biosciences, anti-p53 (clone 1C12) were from Cell Signaling and anti-Rac1 (clone 23A8) were from Millipore.

513 **Flow cytometry and cell sorting**

514 For flow cytometry analysis, single-cell suspensions from thymus, spleen, lymph nodes and
515 bone marrows were incubated with diluted eBioscience™ Fixable Viability Dye eFluor™ 780
516 (ThermoFisher) in phosphate-buffered saline (PBS) prior staining with fluorochrome-
517 conjugated antibodies. Intracellular staining was performed after cell fixation with 4% para-
518 formaldehyde (PFA) by incubating the cells with conjugated antibodies in permeabilization
519 buffer (Thermo Fisher Scientific). For the phenotyping of DN subsets, thymocytes were stained
520 with an anti-lineage cocktail (anti-Gr1, anti-CD11b, anti-CD11c, anti-Ter119, anti-CD3, anti-
521 B220, anti-NK1.1 and anti-TCRγδ) and with anti-CD8α and anti-CD4 antibodies. Data
522 acquisition was performed on a BD LSRII flow cytometer and analysis with the FlowJo
523 software.
524 For DN3 cell purification, thymocytes were first immunomagnetically depleted of CD3, CD4
525 or CD8α positive cells. $Lin^-CD44^-CD25^+CD5^-$ or $Lin^-CD44^-CD25^+CD71^-$ DN3 cells were
526 sorted on a BD FACS Aria cell sorter. For peripheral T cells isolation, total CD4+ T cells and
527 CD8+ T cells were purified from ACK-treated pooled lymph nodes and spleen by magnetic
528 immunodepletion of $CD8^+$, $B220^+$, $MHCII^+$, $NK1.1^+$, $Fc\gamma^+$ and $CD11b^+$ cells and $CD4^+$, $B220^+$,
529 $MHCII^+$, $NK1.1^+$, $Fc\gamma^+$ and $CD11b^+$ cells, respectively.

530

531 **Cell culture**

532 For OP9-DL1 cells co-cultures, OP9-DL1 cells (41) were seeded at 8000 cells per well in 48-
533 well plates and incubated for 24 hours in OP9 culture media (alpha-MEM, 20% FCS, Penicillin
534 and Streptomycin), followed by addition of 100,000 sorted $CD5^-$ or $CD71^-$ DN3 thymocytes
535 per well together with 10 ng/ml recombinant mouse IL-7 (PeproTech).

For proliferation analysis, CD5$^-$ DN3 thymocytes, CD4+ and CD8+ lymph nodes T cells were labeled with 2 µM CTV (Thermo Fisher Scientific) for 15 min at 37 °C. Thymocytes were cultured with OP9-DL1 cells and peripheral T cells were incubated with the indicated doses of anti-CD3 antibodies and with 2µg/ml anti-CD28 antibodies for 48 and 72 hours. For apoptosis analysis, thymocytes and CD4+ T cells were stained with CTV and stimulated for 48 hours as described for proliferation analysis. After stimulation, cells were stained with fluorochrome-conjugated annexin-5 (BD Biosciences) in annexin-5 binding buffer (BD Biosciences). For cell cycle analysis, thymocytes and CD4+ T cells were stimulated for 48 hours as indicated above. Cells were fixed with 4% para-formaldehyde (PFA) and incubated with permeabilization buffer prior staining with DAPI in PBS.

Image stream flow cytometry

For the analysis of the G2/M population, CD4+ T cells were stimulated with 10µg/ml of anti-CD3 antibodies with 2µg/ml of anti-CD28 antibodies for 24 hours. Cells were synchronized by addition of nocodazole (Sigma Aldrich) at 100ng/ml for 18h. Cells were then washed in RPMI supplemented with 10% FCS and incubated with 10 µM of MG132 (Sigma Aldrich) for 3h. Cells were incubated with Fixable Viability Dye prior staining with fluochrome-conjugated anti-CD4 antibodies and DAPI and acquired on an ImageStreamX appartus from Millipore.

Data were analyzed using the IDEAS analysis software from Millipore. We used the "Bright Detail Intensity" (BDI) parameter to discriminate mitotic cells from cells in the G2 phase. This parameter calculates the intensity of the bright pixels after subtraction of the background noise from the images. Cells in mitosis having condensed DNA will present a homogeneously bright staining leading to higher BDI value than cells in the G2 phase with uncondensed DNA. To

559 evaluate cells in metaphase, we used the parameter "Elongatedness" which calculates the length
560 to width ratio on a predefined DAPI mask. Cells with an "Elongatedness" value exeeding 1.5
561 were characterized as cells in metaphase.

562

563 **Immunization with ovalbumin**

564 CD45.1+ CD4+ T cells were purified from lymph nodes and splenocytes from *Lis1*$^{flox/flox}$ and
565 *CD4-Cre Lis1*$^{flox/flox}$ mice expressing the OT2 TCR. 2x10^6 cells in PBS were injected i.v. into
566 C57BL/6J mice (CD45.2$^+$) one hour before immunization with 40 µg of ovalbumin emulsified
567 with RIBI (Sigma Adjuvant System). CD4$^+$ T cell populations from the spleen were analyzed
568 2 and 3 days after immunization.

569

570 **Confocal analysis**

571 CD4+ T cells were labeled with CTV and incubated with 10 µg/ml of anti-CD3 antibodies and
572 2µg/ml of anti-CD28 antibodies for 48 hours. The CTV^{hi}FSC^{lo} (non-proliferating, non-
573 activated) and CTV^{hi}FSC^{hi} (non-proliferating, activated) populations were sorted by flow
574 cytometry. Lin$^-$CD44$^-$CD25$^+$CD5^{hi} thymocytes were sorted by flow cytometry. Cells were
575 deposited on 0.01% poly-L-lysine adsorbed slides (Sigma aldrich), fixed with 4% PFA and
576 permeabilized in PBS containing 0.1% Saponin (Sigma Aldrich). α- and γ-tubulin staining was
577 made in PBS containing 0.1% Saponin, 3% Bovin serum albumin (BSA) and 10mM HEPES at
578 4°C for 18h and revealed with fluorochrome-conjugated anti-mouse and IgG1 and IgG2b
579 antibodies (Thermo Fisher Scientific) for 1 hour at room temperature. DNA was stained with
580 DAPI for 15 min at room temperature in PBS. The slides were then mounted with DABCO

581 solution (Sigma Aldrich) and the images were acquired with an LSM710 confocal microscope
582 equipped with a 63× 1.4 NA objective (Zeiss).

583 For video microscopy, CD4+ T cells were cultured with 10 μg/ml of anti-CD3 and 2 μg/ml of
584 anti-CD28 antibodies on a chambered glass coverslip (IBIDI) for 24 hours. To stain DNA,
585 Hoechst 33342 (Sigma-Aldrich) was added to the culture at a final concentration of 50ng/ml.
586 Cells were observed for 18 hours in a chamber at 37°C and 5% CO2 with a Spinning disk
587 confocal microscope. The z-stack images were edited into film and analyzed using ImageJ.

588

589 **Immunoprecipitation and Western blot analysis**

590 For immunoprecipitation, CD4+ T cells were resuspended in 2 ml of ice-cold lysis buffer (10
591 mM tris-HCl pH 7.4, 150 mM NaCl, 1% Triton, 2 mM Na_3VO_4, 5 mM NaF, 1 mM EDTA, and
592 protease inhibitor cocktail tablet (Roche)) and incubated for 20 min on ice. Lysates were cleared
593 by centrifugation at 18,000g for 15 min at 4°C, and the dynein intermediate chain (DIC) was
594 subjected to immunoprecipitation from cleared lysates for 2 hours at 4°C with 15 μl of protein
595 G–Sepharose resin coated with 12 μg of polyclonal rabbit anti-DIC antibodies. The resin was
596 washed three times and incubated for 10 min at 95°C with Laemmli buffer. For p53 analysis,
597 CD4+ T cells were stimulated with 10 μg/ml of anti-CD3 and 2 μg/ml of anti-CD28 antibodies
598 for 24 and 48 hours and were suspended in ice-cold lysis buffer after each time point. Proteins
599 were resolved by SDS-PAGE and transferred to PVDF membranes according to standard
600 protocols. Membranes were blocked with 5% milk in tris-buffered saline containing Tween at
601 0.05% for 1 hour at room temperature before being incubated with primary antibodies at 4°C
602 overnight. After washing, membranes were incubated with secondary antibodies for 1 hour at
603 room temperature. Subsequently, membranes were incubated with enhanced

chemiluminescence solution (Sigma) for 5 min in the dark, and luminescence was captured with a Bio-Rad XRS+ imager.

Statistical analysis

GraphPad Prism was used to perform statistical analysis. All values in the paper are presented as mean ± SD. Except when indicated, statistical significance was calculated by unpaired two-tailed Mann-Whitney *t* test. *p<0,05 **p<0,001 ***p<0,0001 ****P < 0.0001.

Data availability

All data generated or analyzed during this study are included in the manuscript and supporting files. Source data files have been provided for Figures 1, 2, 3 ,4, 5, and 6 as well as for Figure 1 – Figure supplement 1, Figure 3 – Figure supplement 1 and Figure 3 – Figure supplement 2.

Aknowledgments

The authors thank Loïc Dupré for helpful comments and suggestions and Dr. Deanna Smith for providing Lis1$^{flox/flox}$ mice. We acknowledge the technical assistance provided by the personnel of INSERM US006 Anexplo/creffre animal facility. The authors thank Fatima-Ezzahra L'Faqihi-Olive and Anne-Laure Iscache from the cytometry facility of INFINITy as well as Sophie Allart and Astrid Canivet from the cell imaging facility of INFINITy. Funding: This work was supported by INSERM; the Foundation ARSEP; the Association pour la Recherche sur le Cancer (ARC); the Agence Nationale de la Recherche (ANR-20-CE15-0002); the French Ministry of Higher Education and Research (PhD fellowship for J.A. and S.M.). Competing interests: The authors declare that they have no competing interests. Data and materials availability: All data needed to evaluate the conclusions of the paper are present in the paper or the Supplementary Materials.

Figure and video legends

Figure 1. LIS1 is required for T cell development following the β-selection checkpoint. Phenotypic analyses of thymocytes from *Lis1*$^{flox/flox}$ and *CD2-Cre Lis1*$^{flox/flox}$ mice. (A) Dot plots show CD4 versus CD8 surface staining on thymocytes from *Lis1*$^{flox/flox}$ and *CD2-Cre Lis1*$^{flox/flox}$ mice. Histogram bars represent the numbers of thymocytes in each indicated subset from mice of the indicated genotype. Data are mean ± S.D. and represent a pool of four independent experiments each including n=3-4 mice per group. (B) Dot plots show CD44 versus CD25 surface staining on CD4-CD8- [DN] thymocytes from *Lis1*$^{flox/flox}$ and *CD2-Cre Lis1*$^{flox/flox}$ mice. Histogram bars represent the numbers of thymocytes in each indicated subset from mice of the indicated genotype. Data are mean ± S.D. and represent a pool of five independent experiments each including n=4-5 mice per group. (C) Dot plots show CD27 versus TCRβ intracellular staining on DN3 thymocytes from *Lis1*$^{flox/flox}$ and *CD2-Cre Lis1*$^{flox/flox}$ mice. Histogram bars represent the percentages of TCRβ^{hi}CD27^{hi} thymocytes in DN3 thymocytes. Data are mean ± S.D. and represent a pool of two independent experiments each including n=2-3 mice per group. (D) Dot plots show CD5 versus TCRβ intracellular staining on DN3 thymocytes from *Lis1*$^{flox/flox}$ and *CD2-Cre Lis1*$^{flox/flox}$ mice. Histogram bars represent the percentages of TCRβ^{hi}CD5^{hi} thymocytes in DN3 thymocytes and the MFI of TCRβ and CD5 in DN3 TCRβ^{hi}CD5^{hi} thymocytes from mice of the indicated genotype. Data are mean ± S.D. and represent a pool of two independent experiments each including n=3 mice per group. (E) Histogram graphs show IL-7R, CD71 surface staining and FSC on DN3 thymocytes expressing the TCRβ chain. Histogram bars represent the MFI of IL-7R, CD71 and FSC in the indicated DN3 thymocytes subsets. Data are mean ± S.D. and represent a pool of two independent experiments each including n=3 mice per group. (F) Histogram graphs show DNA intracellular staining on DN3 thymocytes from the indicated subsets. The percentages represent cells in the G2/M phase of

cell cycle. Histogram bars represent the percentages of DN3 TCRβ^{hi}CD5^{hi} thymocytes in the G2/M phase of cell cycle. Data are mean ± S.D. and represent a pool of three independent experiments each including n=1 mouse per group. Unpaired two-tailed Mann–Whitney t tests were performed for all analysis. **P < 0.01; ***P < 0.001; ****P < 0.0001.

Figure 2. LIS1 is required for the proliferation of immature thymocytes after the β-selection checkpoint. (A) CD5^{lo} DN3 thymocytes from *Lis1*$^{flox/flox}$ and *CD2-Cre Lis1*$^{flox/flox}$ were stained with CTV and stimulated with OP9-Dl1 cells for 48 or 72 hours. The histogram graph shows CTV dilution. Bar graphs represent the proliferation of cells determined by flow cytometry at 24, 48 and 72 hours after stimulation. Data are mean ± S.D. and represent three to seven independent experiments each including n=1-2 pooled mice per group. (B) CD5^{lo} DN3 thymocytes from *Lis1*$^{flox/flox}$ and *CD2-Cre Lis1*$^{flox/flox}$ were stimulated with OP9-Dl1 cells for the indicated periods of time. Dot plots show CD44 versus CD25 surface staining on thymocytes from *Lis1*$^{flox/flox}$ and *CD2-Cre Lis1*$^{flox/flox}$ mice. Data are representative of three independent experiments each including n=1-2 pooled mouse per group. (C) CD71^{lo} DN3 thymocytes from *Lis1*$^{flox/flox}$ and *CD2-Cre Lis1*$^{flox/flox}$ were stimulated with OP9-Dl1 cells for 24 hours. Dot plots show CD5 versus TCRβ intracellular staining on thymocytes. Histogram bars represent the percentages of TCRβ^{hi}CD5^{hi} thymocytes in DN3 thymocytes and the MFI CD5 in DN3 TCRβ^{hi}CD5^{hi} thymocytes from mice of the indicated genotype. Data are mean ± S.D. and represent four independent experiments each including n=1-2 pooled mice per group. (D) CD71^{lo} DN3 thymocytes from *Lis1*$^{flox/flox}$ and *CD2-Cre Lis1*$^{flox/flox}$ were stimulated with OP9-Dl1 cells for 48 hours. Dot plots show CD5 versus CD71 staining on CTV^{hi} thymocytes. Histogram bars represent the percentages of CD71^{hi}CD5^{hi} thymocytes in CTV^{lo} DN3 thymocytes. Data are mean ± S.D. and represent four independent experiments each including n=1-2 pooled mice per group. (E) CD71^{lo} DN3 thymocytes from *Lis1*$^{flox/flox}$ and *CD2-Cre*

683 *Lis1*$^{flox/flox}$ were stimulated with OP9-Dl1 cells for 24 hours. The histogram graph shows BCL-
684 2 intracytoplasmic staining in TCRβ^{lo}CD5^{lo} and TCRβ^{hi}CD5^{hi} thymocyte subsets. Histogram
685 bars represent the MFI of BCL-2 in the indicated DN3 thymocyte subsets. Data are mean ±
686 S.D. and represent three independent experiments each including n=1-2 pooled mice per group.
687 (F) CD71^{lo} DN3 thymocytes from *Lis1*$^{flox/flox}$ and *CD2-Cre Lis1*$^{flox/flox}$ were stimulated with OP9-
688 Dl1 cells for 48 hours. Histogram graphs show DNA intracellular staining on thymocytes from
689 the indicated DN3 subsets. The indicated percentages represent cells in the G2/M phase of cell
690 cycle. Histogram bars represent the percentages of DN3 TCRβ^{hi}CD5^{hi} thymocytes in the G2/M
691 phase of cell cycle. Data are mean ± S.D. and represent six independent experiments each
692 including n=1-2 pooled mice per group. (A) Unpaired two-tailed Welch t tests were performed.
693 (C-E) Unpaired two-tailed Mann–Whitney t tests were performed. *P < 0.05, **P < 0.01.
694
695 **Figure 3. LIS1 is required for the proliferation of CD4+ T cells in response to antigen**
696 **stimulation.** (A) CD4^{+} T cells from *Lis1*$^{flox/flox}$ and *CD4-Cre Lis1*$^{flox/flox}$ were stained with CTV
697 and stimulated with anti-CD3 and anti-CD28 antibodies or with PMA and ionomycin (P/I) for
698 72 hours. The histogram graphs show CTV dilution. Bar graphs represent the percentages of
699 cells that divided at least one-time (Tot.) or that divided 1, 2 or 3 times (D1, D2, D3) as
700 determined by flow cytometry at 72 hours after stimulation. Data are mean ± S.D. and represent
701 five independent experiments each including n=3 mice per group. (B) CD4^{+} T cells from
702 *Lis1*$^{flox/flox}$ and *CD4-Cre Lis1*$^{flox/flox}$ were stimulated with anti-CD3 and anti-CD28 antibodies for
703 24 hours. Bar graphs represent the percentages of cells expressing CD25 and CD69 as
704 determined by flow cytometry. Data are mean ± S.D. and represent two independent
705 experiments each including n=1-2 mice per group. (C) CD4^{+} and CD8+ T cells from *Lis1*$^{flox/flox}$
706 and *CD4-Cre Lis1*$^{flox/flox}$ were stimulated with anti-CD3 and anti-CD28 antibodies for 48 hours.
707 Histogram graphs show DNA intracellular staining on CD4+ T cells. The indicated percentages

represent cells in the G2/M phase of cell cycle. Histogram bars represent the percentages of CD4+ and CD8+ T cells in the G2/M phase of cell cycle. Data are mean ± S.D. and represent two independent experiments each including n=3 mice per group. (D) $CD8^+$ T cells from *Lis1*$^{flox/flox}$ and *CD4-Cre Lis1*$^{flox/flox}$ were stained with CTV and stimulated with anti-CD3 and anti-CD28 antibodies or with PMA and ionomycin (P/I) for 72 hours. The histogram graph shows CTV dilution. Bar graphs represent the percentages of cells that divided at least one-time (Tot.) or that divided 1, 2 or 3 times (D1, D2, D3) as determined by flow cytometry at 72 hours after stimulation. (E and F) C57BL/6j mice ($CD45.2^+$) were injected i.v. with CTV stained $CD45.1^+CD4^+$ T cells from *OT2-Lis1*$^{flox/flox}$ and *OT2-CD4-Cre Lis1*$^{flox/flox}$ mice. Mice were then immunized with ovalbumine emulsified in RIBI. Proliferation of CD45.1+CD4+ T cells was analyzed at day two and three after immunization. (E) Bar graphs represent the proliferation and numbers of CD45.1+CD4+ T cells as determined by flow cytometry at day two and three after immunization. Data are mean ± S.D. and are representative of one experiment out of two independent experiments each including n=5 mice per group. (F) The histogram graph shows CTV dilution in CD45.1+CD4+ T cells at day 3 after immunization. Histograms overlay shows CD44 surface staining on undivided CD45.1+CD4+ T cells at day 3 after immunization. Data are representative of one experiment out of two independent experiments each including n=5 mice per group. Unpaired two-tailed Mann–Whitney t tests were performed for all analysis. *P < 0.05; **P < 0.01; ***P < 0.001; ****P < 0.0001.

Figure 4. Dysfunctional chromosome alignment in LIS1-deficient CD4+ T cells leads to abortive mitosis and aneuploidy. (A) $CD4^+$ T cells from *Lis1*$^{flox/flox}$ and *CD4-Cre Lis1*$^{flox/flox}$ mice were stimulated with anti-CD3 and anti-CD28 antibodies for 48 hours. Histogram graphs represent the *Bright Detail Intensity* (BDI) feature on $CD4^+$ T cells in the G2/M phase as determined by image stream flow cytometry. Numbers represent the percentages of cells in

mitosis according to the BDI feature. Images represent DAPI staining in BDI^{low} and BDI^{hi} *Lis1*$^{flox/flox}$ $CD4^+$ T cells. Bar graphs represent the percentages of cells in mitosis (M) out of cells in the G2/M phase (n=30000 cells). Data are mean ± S.D. and represent three independent experiments each including n=1 mouse per group. (B) $CD4^+$ T cells from *Lis1*$^{flox/flox}$ and *CD4-Cre Lis1*$^{flox/flox}$ were stimulated with anti-CD3 and anti-CD28 antibodies for 24 hours, synchronized with nocodazole for 18 hours and incubated with MG132 for 3h to induce metaphase arrest. Histogram graphs represent the *Elongatedness* feature on $CD4^+$ T cells in the M phase as determined by image stream flow cytometry. Numbers represent the percentages of cells in metaphase according to *Elongatedness* feature (n=30000 cells). Images represent DAPI staining in *Elongatedness*^{low} and *Elongatedness*^{hi} *Lis1*$^{flox/flox}$ $CD4^+$ T cells. Bar graphs represent the percentages of cells in metaphase out of cells in the M phase. Data are mean ± S.D. and represent three independent experiments each including n=1 mouse per group. (C) Time-lapse microscopy analysis of cell division in $CD4^+$ T cells from *Lis1*$^{flox/flox}$ and *CD4-Cre Lis1*$^{flox/flox}$ stimulated with anti-CD3 and anti-CD28 antibodies. Images represent DNA staining on CD4+ T cells at the indicated times (hours:minutes). White arrows represent cells with uncondensed DNA. Red arrows represent the same cells after chromosomes formation. The top red arrows in the *CD4-Cre Lis1*$^{flox/flox}$ panel are representative of abortive mitosis. The bottom red arrows in the *CD4-Cre Lis1*$^{flox/flox}$ panel are representative of mitosis leading to aneuploidy. Bar graphs represent the time of mitosis per cell. Data are mean ± S.D. and represent three independent experiments each including n=1 mouse per group. (D) Mitosis outcomes in *Lis1*$^{flox/flox}$ and *CD4-Cre Lis1*$^{flox/flox}$ $CD4^+$ T cells stimulated with anti-CD3 and anti-CD28 antibodies. Numbers represent percentages in the different section out of a total of n=62-64 mitosis analyzed. Data represent three independent experiments each including n=1 mouse per group. (E) $CD4^+$ T cells from *Lis1*$^{flox/flox}$ and *CD4-Cre Lis1*$^{flox/flox}$ were stimulated with anti-CD3 and anti-CD28 antibodies for 48 hours. Cells in G2 phase were analyzed by image stream flow cytometry.

Cells stained with DAPI and Bright-field (BF) images are represented. Bar graphs represent the percentages of cells with multilobed nuclei (n=400 cells). Data are mean ± S.D. and represent three independent experiments each including n=1 mouse per group. (A and B) Unpaired two-tailed Welch t tests were performed. (C) Unpaired two-tailed Mann–Whitney t test was performed. *P < 0.05; **P < 0.01; ***P < 0.001; ****P < 0.0001.

Figure 5. Proliferation leads to p53 up-regulation and apoptosis in LIS1-deficient thymocytes and CD4+ T cells. (A) $CD4^+$ T cells from *Lis1*$^{flox/flox}$ and *CD4-Cre Lis1*$^{flox/flox}$ were stained with CTV and stimulated with anti-CD3 and anti-CD28 antibodies for 48 hours. The histogram graphs show annexin-5 staining on CTV^{hi} (top panel) and CTV^{low} (bottom panel) $CD25^+CD4+$ T cells. Bar graphs represent the percentages of annexin5+ cells in the indicated subsets. Data are mean ± S.D. and represent two independent experiments each including n=1-2 mice per group. (B) Total $CD4^+$ and CD8+ T cells from *Lis1*$^{flox/flox}$ and *CD4-Cre Lis1*$^{flox/flox}$ mice were stimulated with anti-CD3 and anti-CD28 antibodies for the indicated times. Total cytoplasmic extracts of the cells were then analyzed by Western blotting with antibodies against p53, Rac1 and GAPDH, the loading controls. Data are representative of two independent experiments. (C) $CD5^{lo}$ DN3 thymocytes from *Lis1*$^{flox/flox}$ and *CD2-Cre Lis1*$^{flox/flox}$ were stained with CTV and stimulated with OP9-Dl1 cells for 48 hours. The histogram graphs show annexin-5 staining on CTV^{hi} (top panel) and CTV^{low} (bottom panel) $CD5^{hi}CD4+$ T cells. Bar graphs represent the percentages of annexin5+ cells in the indicated subsets. Data are mean ± S.D. and represent two independent experiments each including n=2 mice per group. (D) Total cytoplasmic extracts of the DN thymocytes were analyzed by Western blotting with antibodies against p53 and Rac1, the loading control. Data are representative of two independent experiments. Unpaired two-tailed Welch t tests were performed in A and C. *P < 0.05; ***P < 0.001.

783

784 **Figure 6. Impaired formation of dynein/dynactin complexes is associated with the loss of**
785 **centrosome integrity and the formation of multipolar spindles in LIS-1 deficient**
786 **thymocytes and CD4+ T cells.** (A) $CD4^+$ T cells from *Lis1*$^{flox/flox}$ and *CD4-Cre Lis1*$^{flox/flox}$ were
787 stained with CTV and stimulated with anti-CD3 and anti-CD28 antibodies for 48 hours. Images
788 represent Maximum Intensity Projection of γ-tubulin and DAPI staining on undivided FSC^{lo}
789 (top panel) and FSC^{hi} (bottom panel) CD4+ T cells. Bar graphs represent the percentages of
790 cells with the indicated number of centrosome in total cells (top graph) or in mitotic cells
791 (bottom graph). Data represent one experiment out of two independent experiments with n=30-
792 50 cells analyzed per group. (B) $CD4^+$ T cells from *Lis1*$^{flox/flox}$ and *CD4-Cre Lis1*$^{flox/flox}$ mice
793 were stained with CTV and stimulated with anti-CD3 and anti-CD28 antibodies for 48 hours.
794 Images represent Maximum Intensity Projection of γ-tubulin and α-tubulin staining on
795 undivided FSC^{hi} CD4+ T cells. Bar graphs represent the size of the pericentriolar region (PCM)
796 based on γ-tubulin staining in mitotic cells with the indicated number of centrosomes. Data
797 represent three experiments with n=16-54 centrosomes analyzed per group. (C) Images
798 represent Maximum Intensity Projection of γ-tubulin and DAPI staining $CD5^{hi}$ DN3
799 thymocytes. Bar graphs represent the percentages of cells with the indicated number of
800 centrosomes in mitotic cells. Data represent one experiment out of two independent
801 experiments with n=30-50 cells analyzed per group. (D) $CD4^+$ T cell extracts from *Lis1*$^{flox/flox}$
802 and *CD4-Cre Lis1*$^{flox/flox}$ mice were subjected to immunoprecipitation (IP) with antibodies
803 specific of the intermediate chain of dynein (DIC) or with an IgG2b isotype control and then
804 analyzed by Western blotting with antibodies specific of the indicated proteins (Dynein heavy
805 chain [DHC]). Data represent one experiment out of two independent experiments. Unpaired
806 two-tailed Mann–Whitney t test was performed. ****$P < 0.0001$.

807

Video 1. Time-lapse microscopy of mitosis in wild-type CD4$^+$ T cells. Time-lapse microscopy analysis of mitosis in CD4$^+$ T cells from wild-type mice stimulated with anti-CD3 and anti-CD28 antibodies. Videos represent DNA staining (right panel) and bright field (left panel) on CD4+ T cells.

Video 2. Time-lapse microscopy of abortive mitosis in Lis1-deficient CD4$^+$ T cells. Time-lapse microscopy analysis of mitosis in CD4$^+$ T cells from *CD4-Cre Lis1$^{flox/flox}$* mice stimulated with anti-CD3 and anti-CD28 antibodies. Videos represent DNA staining (right panel) and bright field (left panel) on CD4+ T cells.

Video 3. Time-lapse microscopy of mitosis with aneuploidy in Lis1-deficient CD4$^+$ T cells. Time-lapse microscopy analysis of mitosis in CD4$^+$ T cells from *CD4-Cre Lis1$^{flox/flox}$* mice stimulated with anti-CD3 and anti-CD28 antibodies. Videos represent DNA staining (right panel) and bright field (left panel) on CD4+ T cells.

Figure 1 – Figure Supplement 1. LIS1 is required for B cell development. (A) Dot plots show TCR versus B220 and CD4 versus CD8 surface staining on splenocytes from *Lis1$^{flox/flox}$* and *CD2-Cre Lis1$^{flox/flox}$* mice. Histogram bars represent the numbers of thymocytes in each indicated subset from mice of the indicated genotype. Data are mean ± S.D. and represent four independent experiments each including n=3-4 mice per group. (B) Dot plots show CD4 versus CD8 surface staining on total thymocytes and CD44 versus CD25 surface staining on CD4-CD8- [DN] thymocytes from *Lis1$^{flox/+}$* and *CD2-Cre Lis1$^{flox/+}$* mice. Histogram bars represent the percentages of thymocytes in each indicated subset from mice of the indicated genotype. Data are mean ± S.D. and represent a pool of two independent experiments each including n=1-2 mice per group. (C) Upper dot plots show B220 versus CD19 on bone marrow cells from

833 *Lis1*$^{flox/flox}$ and *CD2-Cre Lis1*$^{flox/flox}$ mice. Lower dot plots show IgM versus c-Kit staining on
834 B220^{+}CD19^{+} bone marrow cells from *Lis1*$^{flox/flox}$ and *CD2-Cre Lis1*$^{flox/flox}$ mice. Histogram bars
835 represent the numbers of cells in each indicated subset from mice of the indicated genotype.
836 Data are mean ± S.D. and represent two independent experiments each including n=3-4 mice
837 per group. Unpaired two-tailed Mann–Whitney t test were performed. *P < 0.05; **P < 0.01;
838 ***P < 0.001; ****P < 0.0001.
839
840 **Figure 3 – Figure Supplement 1. Normal T cell development in *CD4-Cre Lis1*$^{flox/flox}$ *mice.***
841 Phenotypic analyses of thymocytes from *Lis1*$^{flox/flox}$ and *CD4-Cre Lis1*$^{flox/flox}$ mice. (A) Dot plots
842 show CD4 versus CD8 surface staining on thymocytes from *Lis1*$^{flox/flox}$ and *CD4-Cre Lis1*$^{flox/flox}$
843 mice. Histogram bars represent the numbers of thymocytes in each indicated subset from mice
844 of the indicated genotype. Data are mean ± S.D. and represent two independent experiments
845 each including n=2-3 mice per group. (B) Dot plots show CD24 versus TCRβ surface staining
846 on CD4+ SP and CD8+ SP thymocytes from *Lis1*$^{flox/flox}$ and *CD4-Cre Lis1*$^{flox/flox}$ mice.
847 Histogram bars represent the numbers of thymocytes in the indicated subset from mice of the
848 indicated genotype. Data are mean ± S.D. and represent two independent experiments each
849 including n=2 mice per group. (C) Dot plots show CD4 versus CD8 surface staining on
850 thymocytes from *Lis1*$^{flox/flox}$ and *CD4-Cre Lis1*$^{flox/flox}$ mice expressing the AND TCR transgene.
851 Histogram graphs represent the TCR Vα11 surface staining on total thymocytes. Histogram
852 bars represent the numbers of thymocytes in each indicated subset from mice of the indicated
853 genotype. Data are mean ± S.D. and represent two independent experiments each including
854 n=2-3 mice per group. (D) Dot plots show TCR versus B220 and CD4 versus CD8 surface
855 staining on total splenocytes and splenic T cells, respectively, from *Lis1*$^{flox/flox}$ and *CD4-Cre*
856 *Lis1*$^{flox/flox}$ mice. Histogram bars represent the numbers of cells in each indicated subset from
857 mice of the indicated genotype. Data are mean ± S.D. and represent two independent

858 experiments each including n=2-3 mice per group. (E) Dot plots show CD4 versus CD8 surface
859 staining on splenocytes from *Lis1*$^{flox/+}$ and *CD4-Cre Lis1*$^{flox/+}$ mice. Histogram bars represent
860 the numbers of cells in each indicated subset from mice of the indicated genotype. Data are
861 mean ± S.D. and represent two independent experiments each including n=3-4 mice per group.
862 *P < 0.05; **P < 0.01; ***P < 0.001; ****P < 0.0001.
863
864 **Figure 3 – Figure Supplement 2. Effect of LIS1 haploid and diploid deficiency on CD4+**
865 **T-cell proliferation and expansion.** (A) CD4^{+} T cells from *Lis1*$^{flox/+}$ and *CD4-Cre Lis1*$^{flox/+}$
866 were stained with CTV and stimulated with anti-CD3 and anti-CD28 antibodies for 48 hours.
867 The histogram graphs show CTV dilution. Bar graphs represent the percentages of cells that
868 divided at least one-time (Tot.) or that divided 1, 2 or 3 times (D1, D2, D3) as determined by
869 flow cytometry at 72 hours after stimulation. Data are mean ± S.D. and represent two
870 independent experiments each including n=4 mice per group. (B) Total cytoplasmic extracts
871 of CD4^{+} and CD8+ T cells from *Lis1*$^{flox/flox}$ and *CD4-Cre Lis1*$^{flox/flox}$ mice were analyzed by
872 Western blotting with antibodies against LIS1 and GAPDH, the loading control. (C) Bar graphs
873 represent the percentages and numbers of CD45.1+CD4+ T cells as determined by flow
874 cytometry at day seven after immunization. Data are mean ± S.D. and are representative of one
875 experiment including n=5 mice per group. **P < 0.01.
876

877 **References**

878

879 1. Kreslavsky T, Gleimer M, Miyazaki M, Choi Y, Gagnon E, Murre C, et al. beta-
880 Selection-induced proliferation is required for alphabeta T cell differentiation. Immunity.
881 2012;37(5):840-53.
882 2. Penit C, Lucas B, Vasseur F. Cell expansion and growth arrest phases during the
883 transition from precursor (CD4-8-) to immature (CD4+8+) thymocytes in normal and
884 genetically modified mice. J Immunol. 1995;154(10):5103-13.
885 3. Ciofani M, Schmitt TM, Ciofani A, Michie AM, Cuburu N, Aublin A, et al. Obligatory
886 role for cooperative signaling by pre-TCR and notch during thymocyte differentiation. Journal
887 of Immunology. 2004;172(9):5230-9.
888 4. Maillard I, Tu L, Sambandam A, Yashiro-Ohtani Y, Millholland J, Keeshan K, et al.
889 The requirement for Notch signaling at the beta-selection checkpoint in vivo is absolute and
890 independent of the pre-T cell receptor. The Journal of experimental medicine.
891 2006;203(10):2239-45.
892 5. Sprent J, Surh CD. Normal T cell homeostasis: the conversion of naive cells into
893 memory-phenotype cells. Nat Immunol. 2011;12(6):478-84.
894 6. Foulds KE, Zenewicz LA, Shedlock DJ, Jiang J, Troy AE, Shen H. Cutting edge: CD4
895 and CD8 T cells are intrinsically different in their proliferative responses. Journal of
896 Immunology. 2002;168(4):1528-32.
897 7. Seder RA, Ahmed R. Similarities and differences in CD4(+) and CD8(+) effector and
898 memory T cell generation. Nature immunology. 2003;4(9):835-42.
899 8. Chang JT, Palanivel VR, Kinjyo I, Schambach F, Intlekofer AM, Banerjee A, et al.
900 Asymmetric T lymphocyte division in the initiation of adaptive immune responses. Science.
901 2007;315(5819):1687-91.
902 9. Arsenio J, Kakaradov B, Metz PJ, Kim SH, Yeo GW, Chang JT. Early specification of
903 CD8(+) T lymphocyte fates during adaptive immunity revealed by single-cell gene-expression
904 analyses. Nature immunology. 2014;15(4):365-+.
905 10. Bird JJ, Brown DR, Mullen AC, Moskowitz NH, Mahowald MA, Sider JR, et al. Helper
906 T cell differentiation is controlled by the cell cycle. Immunity. 1998;9(2):229-37.
907 11. Ben-Sasson SZ, Gerstel R, Hu-Li J, Paul WE. Cell division is not a "clock" measuring
908 acquisition of competence to produce IFN-gamma or IL-4. Journal of Immunology.
909 2001;166(1):112-20.
910 12. Chang JT, Ciocca ML, Kinjyo I, Palanivel VR, McClurkin CE, De Jong CS, et al.
911 Asymmetric Proteasome Segregation as a Mechanism for Unequal Partitioning of the
912 Transcription Factor T-bet during T Lymphocyte Division. Immunity. 2011;34(4):492-504.
913 13. Nish SA, Zens KD, Kratchmarov R, Lin WHW, Adams WC, Chen YH, et al. CD4(+)
914 T cell effector commitment coupled to self-renewal by asymmetric cell divisions. Journal of
915 Experimental Medicine. 2017;214(1):39-47.
916 14. Cobbold SP, Adams E, Howie D, Waldmann H. CD4(+) T Cell Fate Decisions Are
917 Stochastic, Precede Cell Division, Depend on GITR Co-Stimulation, and Are Associated With
918 Uropodium Development. Frontiers in immunology. 2018;9.
919 15. Markus SM, Marzo MG, McKenney RJ. New insights into the mechanism of dynein
920 motor regulation by lissencephaly-1. Elife. 2020;9.
921 16. Yingling J, Youn YH, Darling D, Toyo-Oka K, Pramparo T, Hirotsune S, et al.
922 Neuroepithelial stem cell proliferation requires LIS1 for precise spindle orientation and
923 symmetric division. Cell. 2008;132(3):474-86.

17. Reiner O, Sapir T. LIS1 functions in normal development and disease. Current opinion in neurobiology. 2013;23(6):951-6.
18. Zimdahl B, Ito T, Blevins A, Bajaj J, Konuma T, Weeks J, et al. Lis1 regulates asymmetric division in hematopoietic stem cells and in leukemia. Nature genetics. 2014;46(3):245-+.
19. Yamada M, Toba S, Yoshida Y, Haratani K, Mori D, Yano Y, et al. LIS1 and NDEL1 coordinate the plus-end-directed transport of cytoplasmic dynein. Embo Journal. 2008;27(19):2471-83.
20. Huang J, Roberts AJ, Leschziner AE, Reck-Peterson SL. Lis1 Acts as a "Clutch" between the ATPase and Microtubule-Binding Domains of the Dynein Motor. Cell. 2012;150(5):975-86.
21. Htet ZM, Gillies JP, Baker RW, Leschziner AE, DeSantis ME, Reck-Peterson SL. LIS1 promotes the formation of activated cytoplasmic dynein-1 complexes. Nature cell biology. 2020;22(5):518-+.
22. Elshenawy MM, Kusakci E, Volz S, Baumbach J, Bullock SL, Yildiz A. Lis1 activates dynein motility by modulating its pairing with dynactin. Nature cell biology. 2020;22(5):570-8.
23. Wang S, Ketcham SA, Schon A, Goodman B, Wang Y, Yates J, 3rd, et al. Nudel/NudE and Lis1 promote dynein and dynactin interaction in the context of spindle morphogenesis. Molecular biology of the cell. 2013;24(22):3522-33.
24. McKenney RJ, Huynh W, Tanenbaum ME, Bhabha G, Vale RD. Activation of cytoplasmic dynein motility by dynactin-cargo adapter complexes. Science. 2014;345(6194):337-41.
25. Ayloo S, Lazarus JE, Dodda A, Tokito M, Ostap EM, Holzbaur EL. Dynactin functions as both a dynamic tether and brake during dynein-driven motility. Nat Commun. 2014;5:4807.
26. Urnavicius L, Zhang K, Diamant AG, Motz C, Schlager MA, Yu M, et al. The structure of the dynactin complex and its interaction with dynein. Science. 2015;347(6229):1441-6.
27. Schlager MA, Hoang HT, Urnavicius L, Bullock SL, Carter AP. In vitro reconstitution of a highly processive recombinant human dynein complex. EMBO J. 2014;33(17):1855-68.
28. Young A, Dictenberg JB, Purohit A, Tuft R, Doxsey SJ. Cytoplasmic dynein-mediated assembly of pericentrin and gamma tubulin onto centrosomes. Molecular biology of the cell. 2000;11(6):2047-56.
29. Blagden SP, Glover DM. Polar expeditions--provisioning the centrosome for mitosis. Nature cell biology. 2003;5(6):505-11.
30. Quintyne NJ, Schroer TA. Distinct cell cycle-dependent roles for dynactin and dynein at centrosomes. Journal of Cell Biology. 2002;159(2):245-54.
31. Zvezdova E, Mikolajczak J, Garreau A, Marcellin M, Rigal L, Lee J, et al. Themis1 enhances T cell receptor signaling during thymocyte development by promoting Vav1 activity and Grb2 stability. Science signaling. 2016;9(428):ra51.
32. Garreau A, Blaize G, Argenty J, Rouquie N, Tourdes A, Wood SA, et al. Grb2-Mediated Recruitment of USP9X to LAT Enhances Themis Stability following Thymic Selection. J Immunol. 2017;199(8):2758-66.
33. Moon HM, Youn YH, Pemble H, Yingling J, Wittmann T, Wynshaw-Boris A. LIS1 controls mitosis and mitotic spindle organization via the LIS1-NDEL1-dynein complex. Hum Mol Genet. 2014;23(2):449-66.
34. Ngoi SM, Lopez JM, Chang JT. The Microtubule-Associated Protein Lis1 Regulates T Lymphocyte Homeostasis and Differentiation. J Immunol. 2016.
35. Greaves DR, Wilson FD, Lang G, Kioussis D. Human CD2 3'-flanking sequences confer high-level, T cell-specific, position-independent gene expression in transgenic mice. Cell. 1989;56(6):979-86.

974 36. Boudil A, Matei IR, Shih HY, Bogdanoski G, Yuan JS, Chang SG, et al. IL-7
975 coordinates proliferation, differentiation and Tcra recombination during thymocyte beta-
976 selection. Nature immunology. 2015;16(4):397-405.
977 37. Azzam HS, Grinberg A, Lui K, Shen H, Shores EW, Love PE. CD5 expression is
978 developmentally regulated by T cell receptor (TCR) signals and TCR avidity. Journal of
979 Experimental Medicine. 1998;188(12):2301-11.
980 38. Taghon T, Yui MA, Pant R, Diamond RA, Rothenberg EV. Developmental and
981 molecular characterization of emerging beta- and gammadelta-selected pre-T cells in the adult
982 mouse thymus. Immunity. 2006;24(1):53-64.
983 39. Ciofani M, Zuniga-Pflucker JC. Notch promotes survival of pre-T cells at the beta-
984 selection checkpoint by regulating cellular metabolism. Nature immunology. 2005;6(9):881-8.
985 40. Kelly AP, Finlay DK, Hinton HJ, Clarke RG, Fiorini E, Radtke F, et al. Notch-induced
986 T cell development requires phosphoinositide-dependent kinase 1. Embo J. 2007;26(14):3441-
987 50.
988 41. Schmitt TM, de Pooter RF, Gronski MA, Cho SK, Ohashi PS, Zuniga-Pflucker JC.
989 Induction of T cell development and establishment of T cell competence from embryonic stem
990 cells differentiated in vitro. Nature immunology. 2004;5(4):410-7.
991 42. Akashi K, Kondo M, von Freeden-Jeffry U, Murray R, Weissman IL. Bcl-2 rescues T
992 lymphopoiesis in interleukin-7 receptor-deficient mice. Cell. 1997;89(7):1033-41.
993 43. Maraskovsky E, OReilly LA, Teepe M, Corcoran LM, Peschon JJ, Strasser A. Bcl-2
994 can rescue T lymphocyte development in interleukin-7 receptor-deficient mice but not in
995 mutant rag-1(-/-) mice. Cell. 1997;89(7):1011-9.
996 44. Kastenhuber ER, Lowe SW. Putting p53 in Context. Cell. 2017;170(6):1062-78.
997 45. Nigg EA, Stearns T. The centrosome cycle: Centriole biogenesis, duplication and
998 inherent asymmetries. Nature cell biology. 2011;13(10):1154-60.
999 46. Holland AJ, Cleveland DW. Boveri revisited: chromosomal instability, aneuploidy and
1000 tumorigenesis. Nature reviews Molecular cell biology. 2009;10(7):478-87.
1001 47. Maiato H, Logarinho E. Mitotic spindle multipolarity without centrosome amplification.
1002 Nature cell biology. 2014;16(5):386-U23.
1003 48. Reck-Peterson SL, Redwine WB, Vale RD, Carter AP. The cytoplasmic dynein
1004 transport machinery and its many cargoes (vol 19, pg 382, 2018). Nat Rev Mol Cell Bio.
1005 2018;19(7):479-.
1006 49. Jung HR, Song KH, Chang JT, Doh J. Geometrically Controlled Asymmetric Division
1007 of CD4+T Cells Studied by Immunological Synapse Arrays. PloS one. 2014;9(3).
1008 50. Daum JR, Potapova TA, Sivakumar S, Daniel JJ, Flynn JN, Rankin S, et al. Cohesion
1009 Fatigue Induces Chromatid Separation in Cells Delayed at Metaphase. Current Biology.
1010 2011;21(12):1018-24.
1011 51. Faulkner NE, Dujardin DL, Tai CY, Vaughan KT, O'Connell CB, Wangs YL, et al. A
1012 role for the lissencephaly gene LIS1 in mitosis and cytoplasmic dynein function. Nature cell
1013 biology. 2000;2(11):784-91.
1014 52. Cimini D, Howell B, Maddox P, Khodjakov A, Degrassi F, Salmon ED. Merotelic
1015 kinetochore orientation is a major mechanism of aneuploidy in mitotic mammalian tissue cells.
1016 Journal of Cell Biology. 2001;153(3):517-27.
1017 53. Barenz F, Mayilo D, Gruss OJ. Centriolar satellites: Busy orbits around the centrosome.
1018 European Journal of Cell Biology. 2011;90(12):983-9.
1019 54. Dammermann A, Merdes A. Assembly of centrosomal proteins and microtubule
1020 organization depends on PCM-1. Journal of Cell Biology. 2002;159(2):255-66.
1021 55. Krauss SW, Spence JR, Bahmanyar S, Barth AIM, Go MM, Czerwinski D, et al.
1022 Downregulation of protein 4.1R, a mature centriole protein, disrupts centrosomes, alters cell

cycle progression, and perturbs mitotic spindles and anaphase. Molecular and cellular biology. 2008;28(7):2283-94.
56. Kim K, Rhee K. The pericentriolar satellite protein CEP90 is crucial for integrity of the mitotic spindle pole. Journal of cell science. 2011;124(Pt 3):338-47.
57. Fu G, Vallee S, Rybakin V, McGuire MV, Ampudia J, Brockmeyer C, et al. Themis controls thymocyte selection through regulation of T cell antigen receptor-mediated signaling. Nature immunology. 2009;10(8):848-56.
58. Lesourne R, Uehara S, Lee J, Song KD, Li L, Pinkhasov J, et al. Themis, a T cell-specific protein important for late thymocyte development. Nature immunology. 2009;10(8):840-7.
59. Johnson AL, Aravind L, Shulzhenko N, Morgun A, Choi SY, Crockford TL, et al. Themis is a member of a new metazoan gene family and is required for the completion of thymocyte positive selection. Nature immunology. 2009;10(8):831-9.
60. Brzostek J, Gautam N, Zhao X, Chen EW, Mehta M, Tung DWH, et al. T cell receptor and cytokine signal integration in CD8(+) T cells is mediated by the protein Themis. Nature immunology. 2020;21(2):186-+.
61. Choi S, Warzecha C, Zvezdova E, Lee J, Argenty J, Lesourne R, et al. THEMIS enhances TCR signaling and enables positive selection by selective inhibition of the phosphatase SHP-1. Nature immunology. 2017.
62. Liu X, Zheng H, Li X, Wang S, Meyerson HJ, Yang W, et al. Gain-of-function mutations of Ptpn11 (Shp2) cause aberrant mitosis and increase susceptibility to DNA damage-induced malignancies. Proceedings of the National Academy of Sciences of the United States of America. 2016;113(4):984-9.
63. Li XL, Liu LS, Li R, Wu AL, Lu JQ, Wu QZ, et al. Hepatic loss of Lissencephaly 1 (Lis1) induces fatty liver and accelerates liver tumorigenesis in mice. Journal of Biological Chemistry. 2018;293(14):5160-71.
64. Xing Z, Tang X, Gao Y, Da L, Song H, Wang SQ, et al. The human LIS1 is downregulated in hepatocellular carcinoma and plays a tumor suppressor function. Biochem Bioph Res Co. 2011;409(2):193-9.
65. Messi E, Florian MC, Caccia C, Zanisi M, Maggi R. Retinoic acid reduces human neuroblastoma cell migration and invasiveness: effects on DCX, LISI, neurofilaments-68 and vimentin expression. Bmc Cancer. 2008;8.
66. Suzuki SO, McKenney RJ, Mawatari S, Mizuguchi M, Mikami A, Iwaki T, et al. Expression patterns of LIS1, dynein and their interaction partners dynactin, NudE, NudEL and NudC in human gliomas suggest roles in invasion and proliferation. Acta Neuropathol. 2007;113(5):591-9.
67. Yang R, Chen YJ, Tang C, Li HB, Wang B, Yan Q, et al. MicroRNA-144 suppresses cholangiocarcinoma cell proliferation and invasion through targeting platelet activating factor acetylhydrolase isoform 1b. Bmc Cancer. 2014;14.
68. Cao SY, Lu XM, Wang LH, Qian XF, Jin GF, Ma HX. The functional polymorphisms of LIS1 are associated with acute myeloid leukemia risk in a Han Chinese population. Leukemia Res. 2017;54:7-11.
69. Hirotsune S, Fleck MW, Gambello MJ, Bix GJ, Chen A, Clark GD, et al. Graded reduction of Pafah1b1 (Lis1) activity results in neuronal migration defects and early embryonic lethality. Nature genetics. 1998;19(4):333-9.

Figure 1

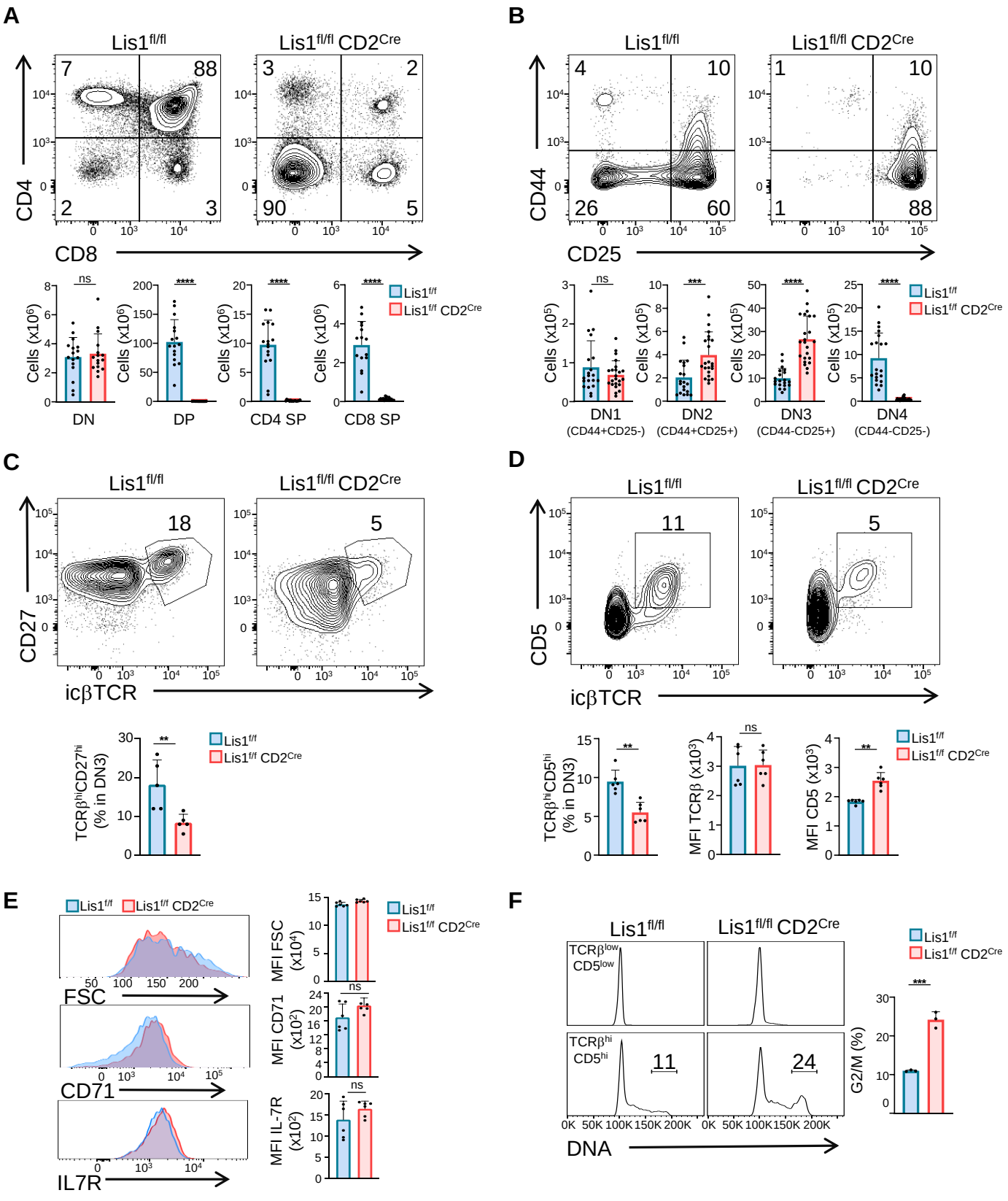
A
Lis1fl/fl
Lis1fl/fl CD2Cre
CD4
CD8
7
88
2
3
3
2
90
5
Cells (x10⁶)
ns
****
DN
DP
CD4 SP
CD8 SP
Lis1f/f
Lis1f/f CD2Cre
B
CD44
CD25
4
10
26
60
1
10
1
88
Cells (x10⁵)
ns
***
****
DN1
(CD44+CD25-)
DN2
(CD44+CD25+)
DN3
(CD44-CD25+)
DN4
(CD44-CD25-)
C
CD27
icβTCR
18
5
TCRβhiCD27hi
(% in DN3)
**
D
CD5
icβTCR
11
5
TCRβhiCD5hi
(% in DN3)
MFI TCRβ (x10³)
MFI CD5 (x10³)
E
FSC
CD71
IL7R
MFI FSC (x10⁴)
MFI CD71 (x10²)
MFI IL-7R (x10²)
F
TCRβlow
CD5low
TCRβhi
CD5hi
11
24
DNA
0K 50K 100K 150K 200K
G2/M (%)
***

Figure 1 - Figure Supplement 1

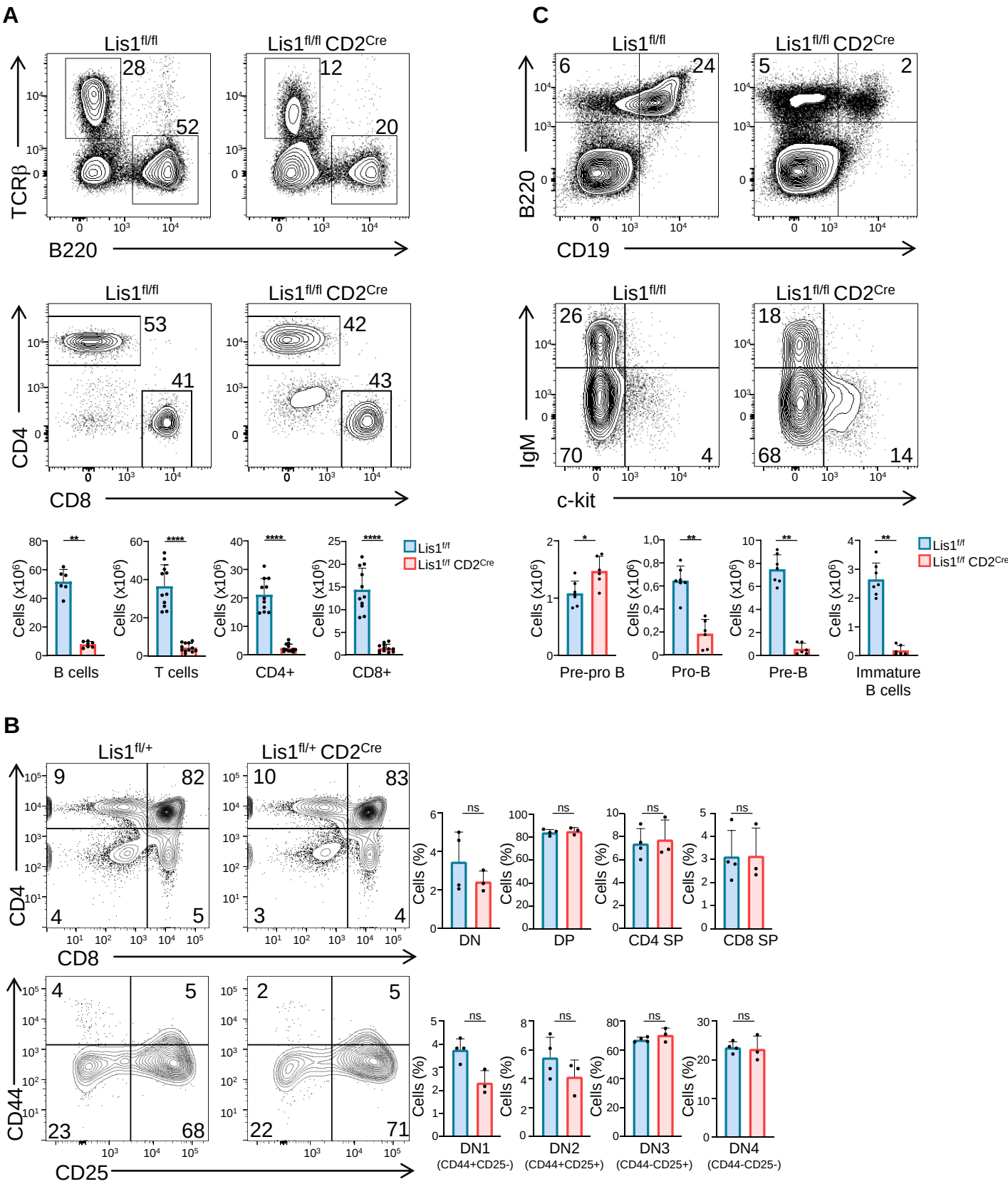

Figure 2

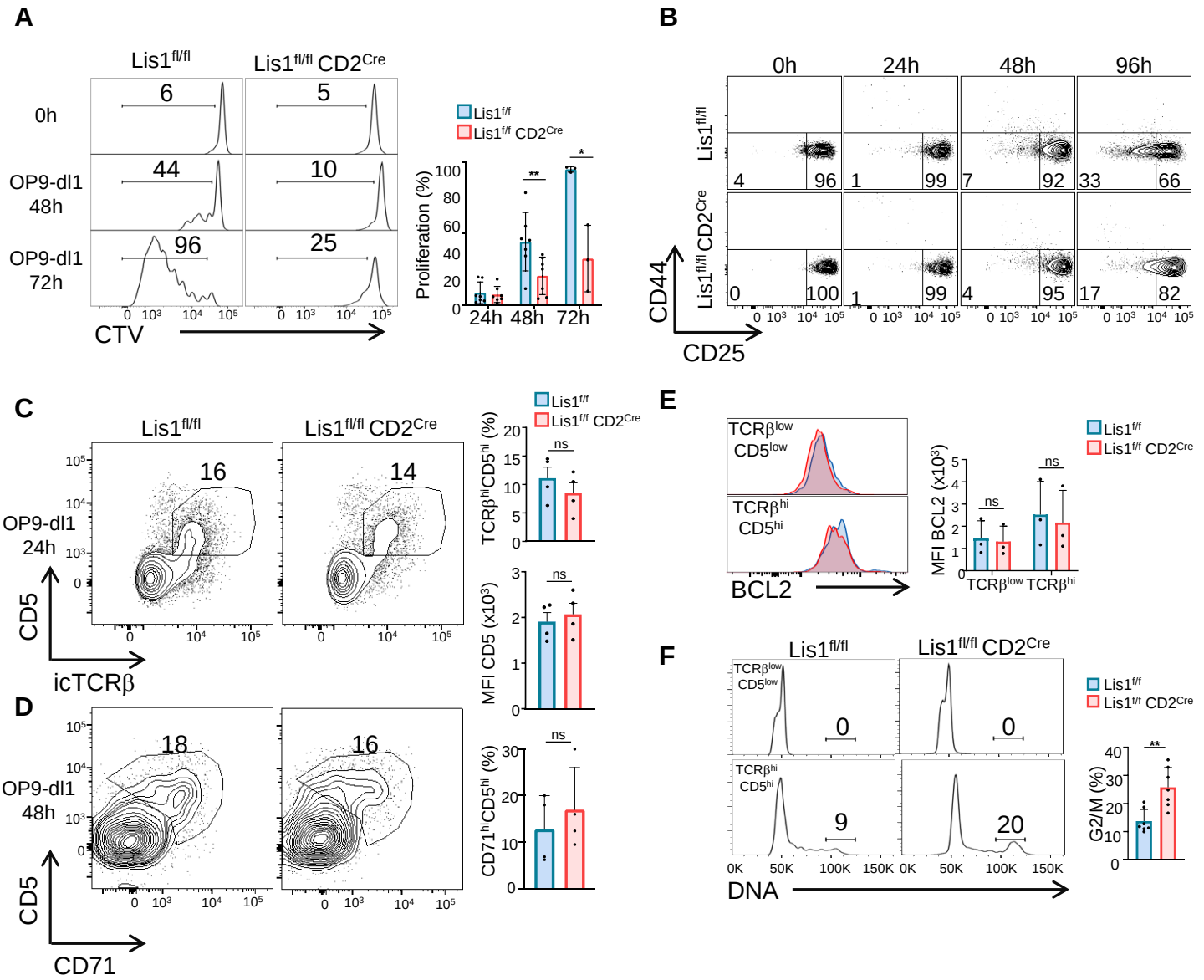
A
Lis1fl/fl
Lis1fl/fl CD2Cre
0h
OP9-dl1 48h
OP9-dl1 72h
6
5
44
10
96
25
CTV
Lis1f/f
Lis1f/f CD2Cre
Proliferation (%)
24h 48h 72h
B
0h
24h
48h
96h
Lis1fl/fl
Lis1fl/fl CD2Cre
4 96
1 99
7 92
33 66
0 100
1 99
4 95
17 82
CD44
CD25
C
Lis1fl/fl
Lis1fl/fl CD2Cre
OP9-dl1 24h
16
14
CD5
icTCRβ
TCRβhiCD5hi (%)
ns
MFI CD5 (x10³)
D
OP9-dl1 48h
18
16
CD71hiCD5hi (%)
CD71
E
TCRβlow CD5low
TCRβhi CD5hi
BCL2
MFI BCL2 (x10³)
TCRβlow TCRβhi
F
TCRβlow CD5low
TCRβhi CD5hi
0
0
9
20
DNA
0K 50K 100K 150K
G2/M (%)
**

Figure 3

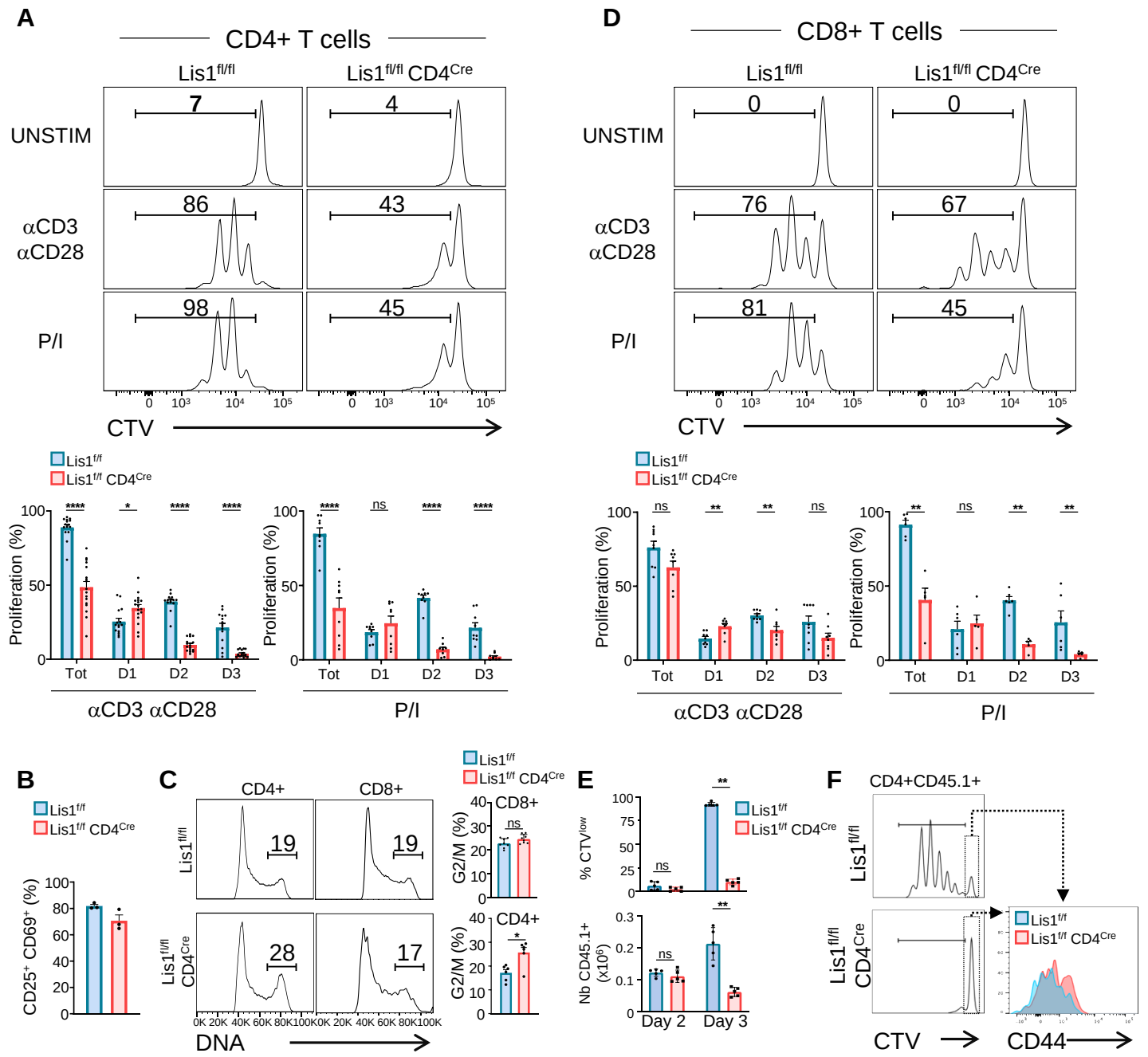
A
CD4+ T cells
Lis1fl/fl
Lis1fl/fl CD4Cre
UNSTIM
αCD3 αCD28
P/I
7
4
86
43
98
45
CTV
Lis1f/f
Lis1f/f CD4Cre
Proliferation (%)
Tot
D1
D2
D3
αCD3 αCD28
P/I
D
CD8+ T cells
0
0
76
67
81
45

B
Lis1f/f
Lis1f/f CD4Cre
CD25+ CD69+ (%)

C
CD4+
CD8+
Lis1fl/fl
Lis1fl/fl CD4Cre
19
19
28
17
DNA
G2/M (%)
ns
*

E
% CTVlow
Nb CD45.1+ (x10⁶)
ns
**
Day 2
Day 3

F
CD4+CD45.1+
Lis1fl/fl
Lis1fl/fl CD4Cre
CTV
CD44

Figure 3 - Figure Supplement 1

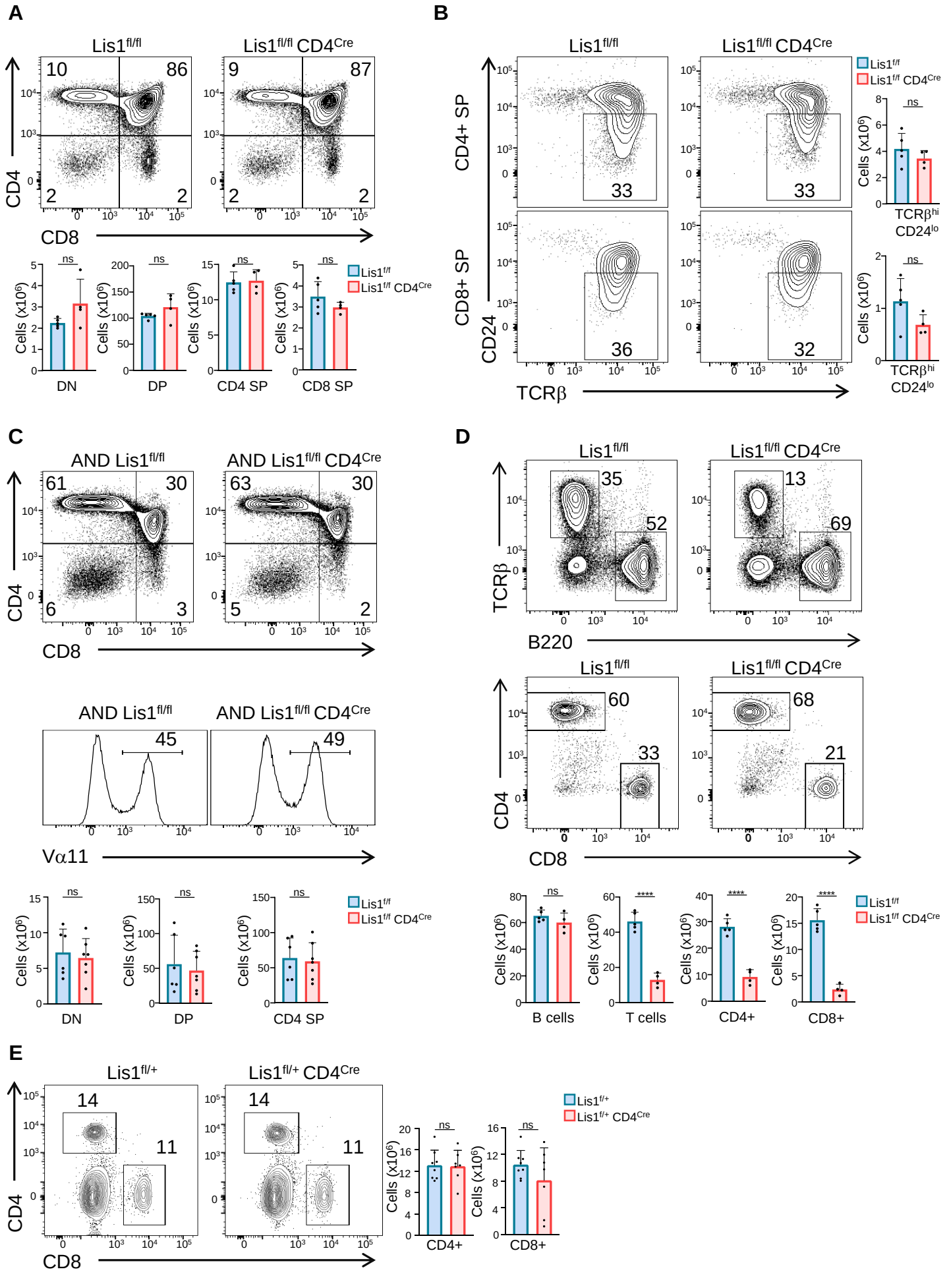

Figure 3 - Figure Supplement 2

A

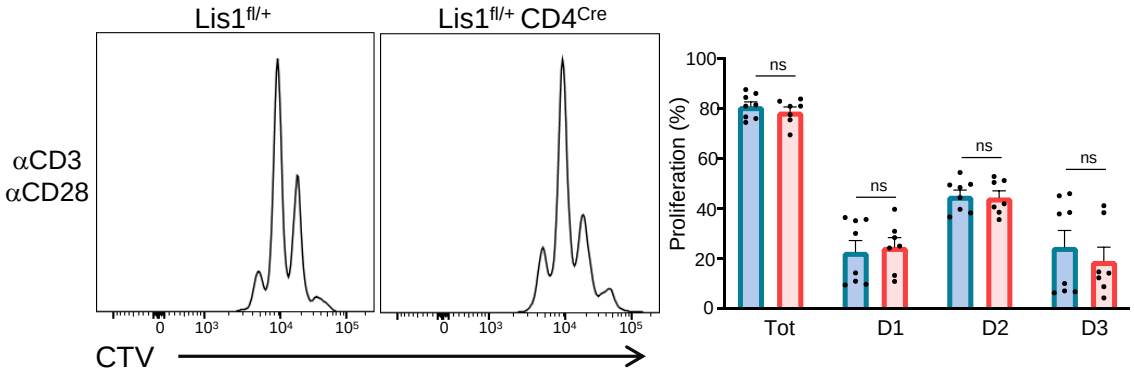

B

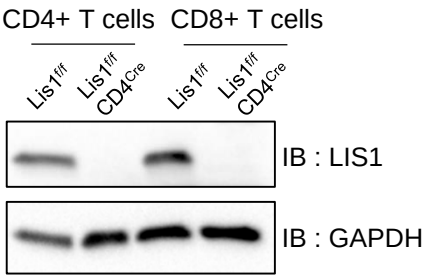

C

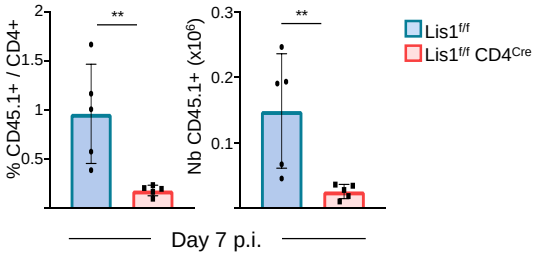

Figure 4

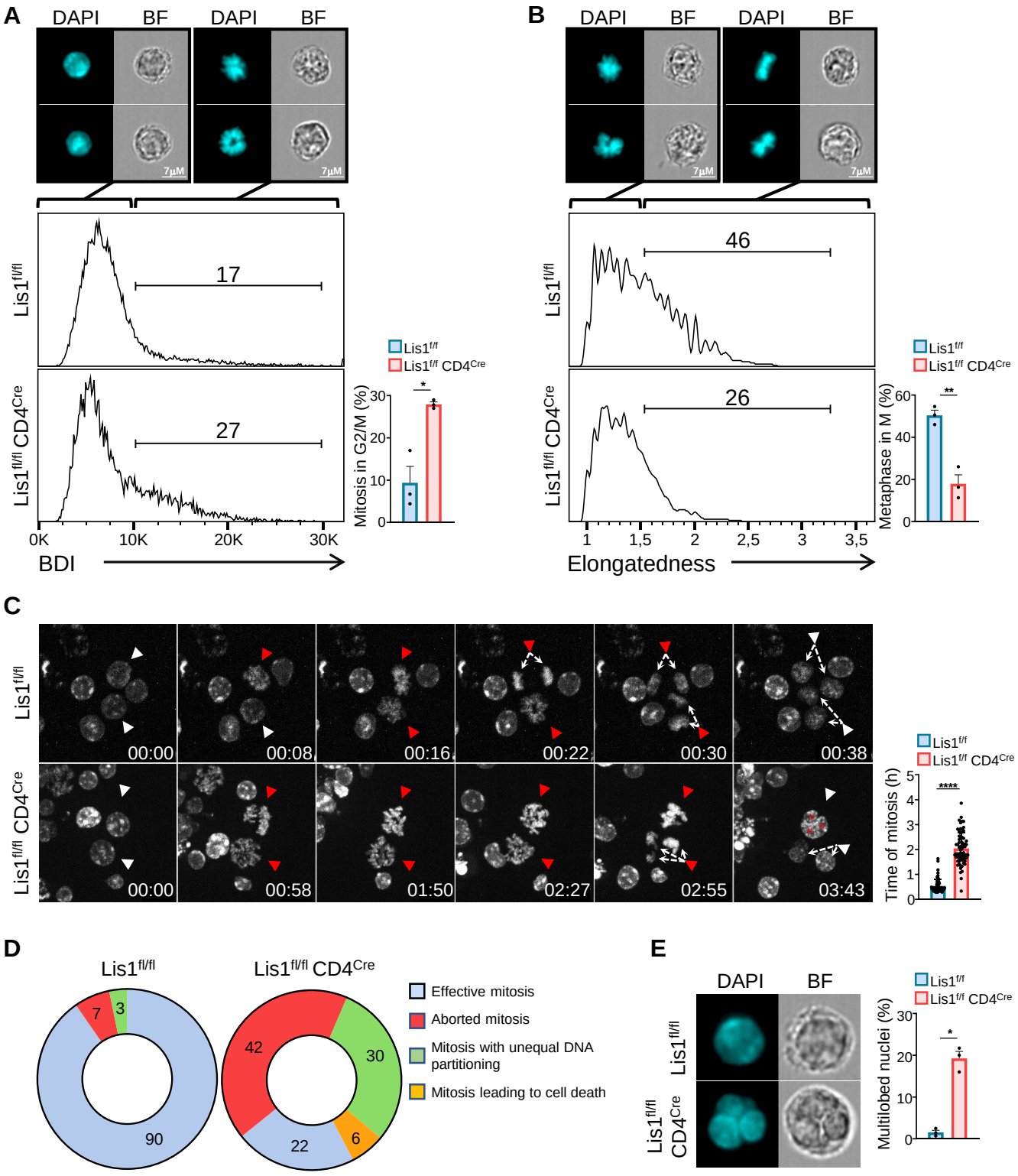
A
DAPI
BF
DAPI
BF
7µM
Lis1f/fl
17
Lis1fl/fl CD4Cre
27
0K
10K
20K
30K
BDI
Lis1f/f
Lis1f/f CD4Cre
Mitosis in G2/M (%)
B
46
26
1
1,5
2
2,5
3
3,5
Elongatedness
Metaphase in M (%)
C
00:00
00:08
00:16
00:22
00:30
00:38
00:58
01:50
02:27
02:55
03:43
Time of mitosis (h)
D
Lis1fl/fl
Lis1fl/fl CD4Cre
7
3
90
42
30
22
6
Effective mitosis
Aborted mitosis
Mitosis with unequal DNA partitioning
Mitosis leading to cell death
E
Multilobed nuclei (%)

Figure 5

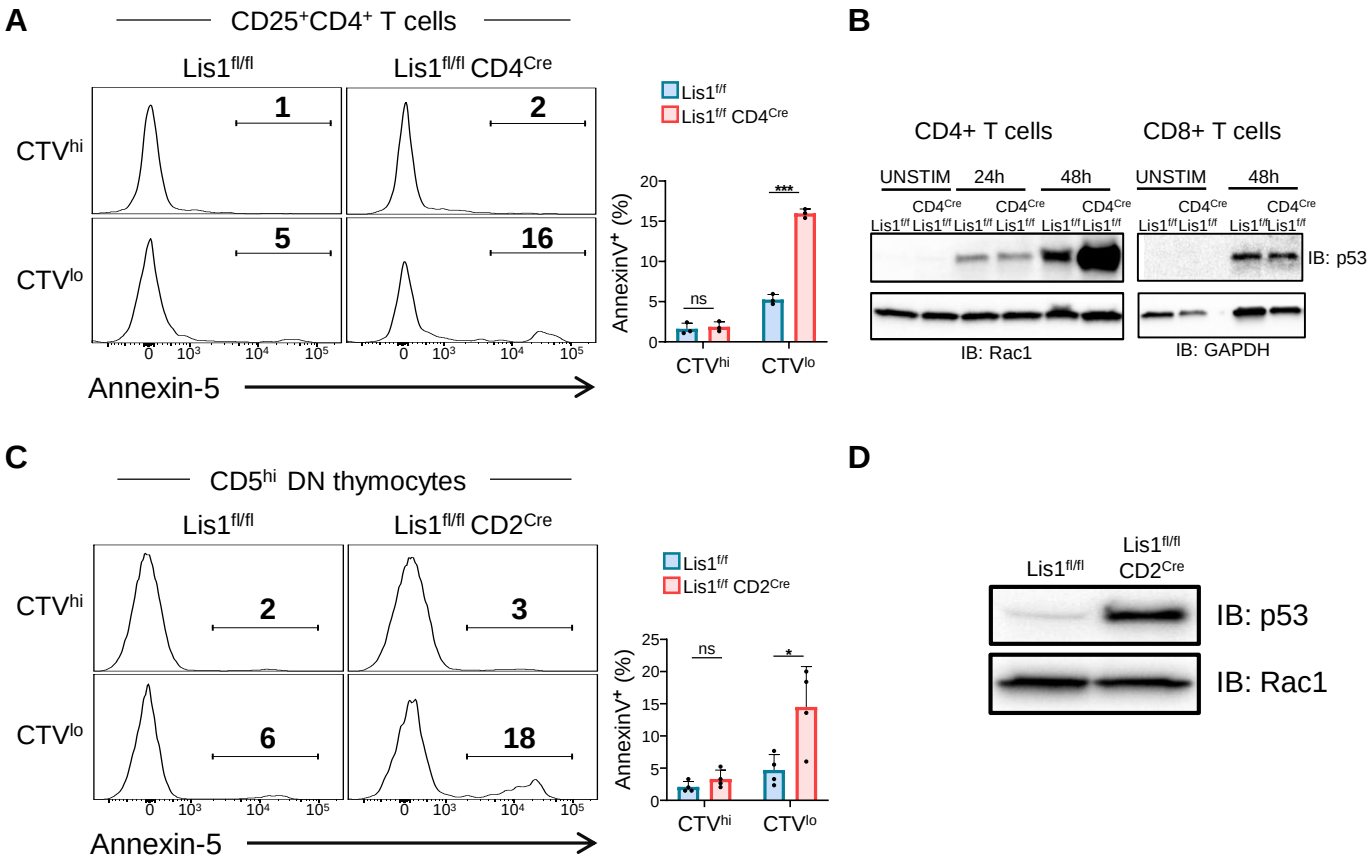
A
CD25+CD4+ T cells
Lis1fl/fl
Lis1fl/fl CD4Cre
CTVhi
CTVlo
1
2
5
16
Annexin-5
Lis1f/f
Lis1f/f CD4Cre
AnnexinV+ (%)
ns
***
CTVhi
CTVlo
B
CD4+ T cells
CD8+ T cells
UNSTIM
24h
48h
IB: p53
IB: Rac1
IB: GAPDH
C
CD5hi DN thymocytes
Lis1fl/fl
Lis1fl/fl CD2Cre
2
3
6
18
Annexin-5
Lis1f/f
Lis1f/f CD2Cre
ns
*
D
Lis1fl/fl
Lis1fl/fl CD2Cre
IB: p53
IB: Rac1

Figure 6

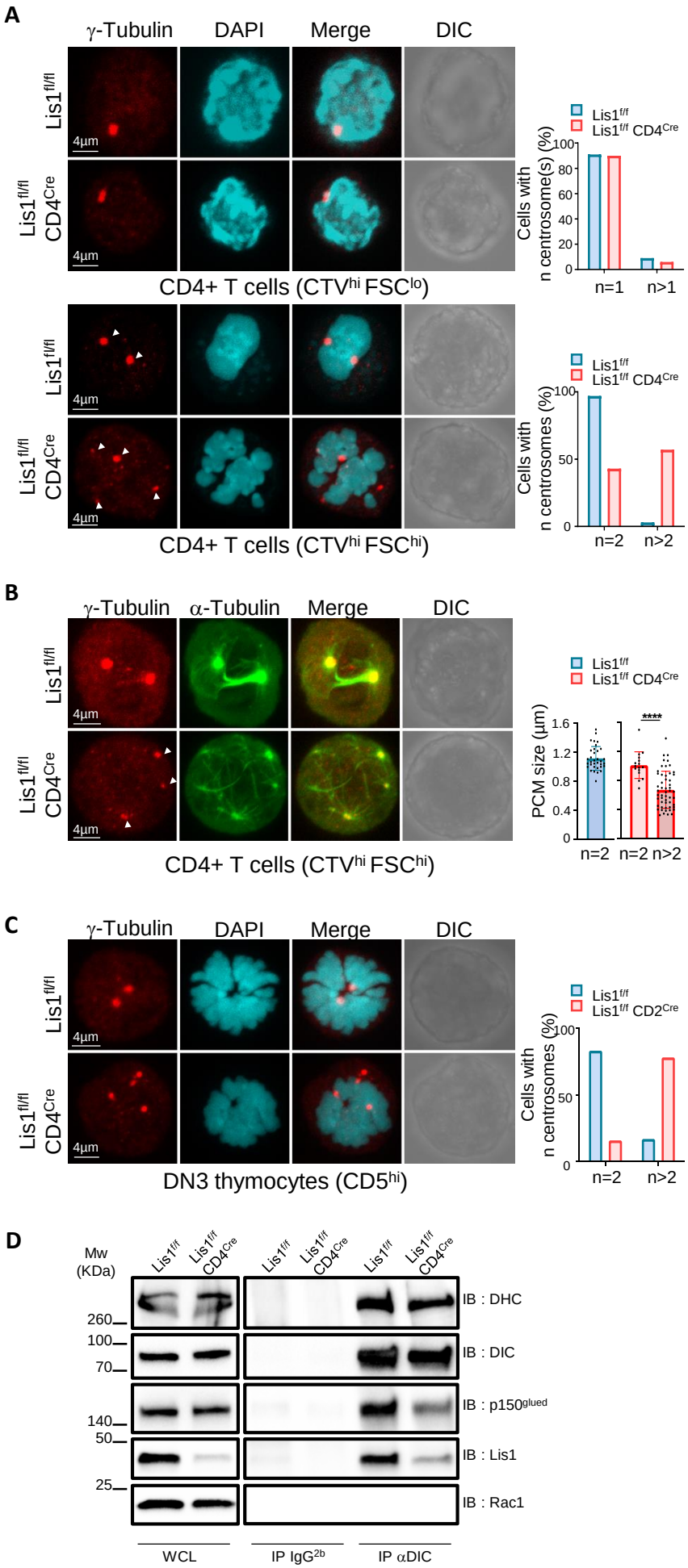
A
γ-Tubulin
DAPI
Merge
DIC
Lis1fl/fl
Lis1fl/fl CD4Cre
4µm
CD4+ T cells (CTVhi FSClo)
CD4+ T cells (CTVhi FSChi)
Lis1f/f
Lis1f/f CD4Cre
Cells with n centrosome(s) (%)
n=1
n>1
Cells with n centrosomes (%)
n=2
n>2
B
α-Tubulin
PCM size (µm)
****
n=2 n>2
C
Lis1f/f CD2Cre
DN3 thymocytes (CD5hi)
D
Mw (KDa)
260
100
70
140
50
25
IB : DHC
IB : DIC
IB : p150glued
IB : Lis1
IB : Rac1
WCL
IP IgG2b
IP αDIC